Drug Design, Development and Therapy

Dovepress
Taylor & Francis Group

Open Access Full Text Article

ORIGINAL RESEARCH

Curcumin Analog J7 Attenuates Liver Fibrosis and Metabolic Dysregulation in a Rat Model of Type 2 Diabetes via Modulation of TGF-β/Smad and NF-κB/BCL-2/BAX Pathways

Jun Ma[1], Wei Chen[2], Deep K Vaishnani[3], Congying Wang[2], Shuman Xue[2], Qiuqin Yang[4], Yuheng Tong[4], Ningjia Lei[5], Zhichao Zhao[6], Furong Ying[7]

[1]Department of Pathology, The First Affiliated Hospital of Wenzhou Medical University, Wenzhou, Zhejiang, 325000, People's Republic of China; [2]Renji College, Wenzhou Medical University, Wenzhou, Zhejiang, 325035, People's Republic of China; [3]School of International Studies, Wenzhou Medical University, Wenzhou, Zhejiang, 325035, People's Republic of China; [4]School of Clinical Medicine, Wenzhou Medical University, Wenzhou, Zhejiang, 325035, People's Republic of China; [5]Pharmacy College, Wenzhou Medical University, Wenzhou, Zhejiang, 325035, People's Republic of China; [6]Department of Critical Care Medicine, Yuyao People's Hospital, Yuyao, Zhejiang, 315400, People's Republic of China; [7]Department of Clinical Laboratory, Key Laboratory of Clinical Laboratory Diagnosis and Translational Research of Zhejiang Province, the First Affiliated Hospital of Wenzhou Medical University, Wenzhou, Zhejiang, 325000, People's Republic of China

Correspondence: Furong Ying, Department of Clinical Laboratory, Key Laboratory of Clinical Laboratory Diagnosis and Translational Research of Zhejiang Province, the First Affiliated Hospital of Wenzhou Medical University, Wenzhou, Zhejiang, 325000, People's Republic of China, Email 764741293@qq.com

Objective: To evaluate the therapeutic potential of the curcumin analog J7 in protecting the liver and regulating glucose and lipid metabolism in rats with type 2 diabetes.

Methods: Bioinformatics methods were used to identify signaling pathways linked to diabetic liver disease. Diabetic rats were treated with curcumin, low-dose J7, or high-dose J7, and liver function and fibrosis were assessed through biochemical analyses, histopathology, immunohistochemistry, and ELISA.

Results: J7 administration significantly improved lisver function, reduced fibrosis, and regulated metabolic profiles in diabetic rats. J7 downregulated TGF-β1, NF-κB p65, and BAX, while upregulating BCL-2, showing superior effects to traditional curcumin in reducing TGF-β1 and inhibiting α-SMA expression.

Conclusion: J7 demonstrates potential as a therapeutic agent for managing liver complications in type 2 diabetes, effectively attenuating liver fibrosis and regulating metabolism through the modulation of key signaling pathways and proteins.

Plain Language Summary: Diabetes is a common condition that can cause serious problems in the liver, such as damage and scarring (fibrosis). These problems are linked to how the body handles sugar and fat. Right now, there are not many effective treatments for diabetes-related liver issues. Our study looked at a new drug called J7, which is based on curcumin, a natural compound found in turmeric, to see if it could help protect the liver and improve sugar and fat metabolism. We used a rat model of type 2 diabetes to test J7. Rats were given either curcumin, a low dose of J7, or a high dose of J7. We then measured how well their livers were working and examined their liver tissue under a microscope. We also looked at the levels of specific molecules in the liver that are involved in inflammation, scarring, and cell survival. We found that J7 worked better than regular curcumin. It reduced liver damage, improved how the liver handled sugar and fat, and lessened scarring. J7 achieved this by affecting certain biological pathways, like the TGF-β/Smad pathway and NF-κB signaling, which are key players in liver damage and inflammation. These results suggest that J7 could be a promising new treatment for liver problems in people with diabetes. This study highlights the potential of improving natural compounds like curcumin to make them more effective as medicines. Further research is needed to explore how J7 might help people with diabetes and liver issues.

Keywords: insulin resistance, metabolic dysfunction-associated fatty liver disease, MAFLD, curcumin analog, liver fibrosis, TGF-β/Smad signaling pathway, NF-κB-BCL-2/BAX axis

Received: 20 December 2024
Accepted: 23 March 2025
Published: 1 April 2025

Introduction

Insulin signaling is crucial in regulating blood sugar levels, inhibiting glucose production, and promoting fatty acid synthesis in the liver. Genetic susceptibility, either alone or combined with environmental factors, is a significant risk factor for type 2 diabetes (T2D), a multifactorial disease characterized by obesity and insulin resistance. Insulin resistance or overnutrition can lead to or contribute to metabolic dysfunction-associated fatty liver disease (MAFLD).[1]

The primary feature of MAFLD is the accumulation of triacylglycerol in the liver.[2] Dyslipidemia and liver lipid accumulation are major factors in this condition. Notably, a significant and independent correlation exists between liver fatty degeneration (rather than fibrosis or inflammation) and insulin resistance in MAFLD patients.[3] Intrahepatic fat, rather than visceral fat, correlates with insulin resistance in the liver, skeletal muscle, and adipose tissue.[4] Adipose tissue inflammation leads to insulin resistance, with liver insulin resistance being the initial event preceding peripheral tissue insulin resistance. Managing T2D involves lifestyle changes and therapies aimed at controlling hyperglycemia, insulin levels, and improving insulin signaling. However, there are no approved drugs specifically for MAFLD, underscoring the need for safer alternatives for both MAFLD and T2D.

Curcumin, an active compound from turmeric (Curcuma longa), has anti-cancer, anti-inflammatory, anti-oxidant, and anti-viral properties.[5,6] Some studies suggest that curcumin can prevent insulin resistance and obesity-related complications.[7] Efforts to improve curcumin's bioavailability and efficacy have led to the development of various curcumin analogs.[8] These analogs show better in vitro stability and improved pharmacokinetic profiles, offering potential alternatives to curcumin.[9,10]

Materials and Methods

Integration of Network Pharmacology with Molecular Docking Technology

In the present study, we adopted a systematic approach to identify potential therapeutic targets for Curcumin J7 by utilizing five distinct databases. Initially, we accessed the Traditional Chinese Medicine Integrated Database (TCMID) at http://www.megabionet.org/tcmid/ and performed a comprehensive search using the keywords "Curcumin" and "J7".[11] This search allowed us to extract pharmacological effects and relevant target information associated with Curcumin J7, compiling potential targets from pertinent literature. Subsequently, we consulted the Encyclopedia of Traditional Chinese Medicine (ETCM) database at http://www.tcmip.cn/ETCM, repeating the search with a focus on elucidating the pharmacological effects and molecular mechanisms of Curcumin J7, and curated additional potential targets from the available literature.[12]

Following the data collection from TCM-specific resources, we turned to the SwissTargetPrediction database at http://swisstargetprediction.ch,[13] where we input the chemical structure or SMILES string of Curcumin J7, selected human as the species for prediction, and filtered targets with a probability greater than zero for further examination. Lastly, we explored the Comparative Toxicogenomics Database (CTD) at https://ctdbase.org/, utilizing "Curcumin" and "J7" as search terms to retrieve chemical-gene interaction data relevant to Curcumin.[14] Analyzing this data enabled us to extract additional potential targets for Curcumin J7. In addition, a search in the PubMed database at https://pubmed.ncbi.nlm.nih.gov/ using "Curcumin" and "J7" allowed us to identify pertinent literature, focusing on articles that provided information on curcumin targets. After gathering data from all the above databases, we systematically organized and deduplicated the target information to ensure data integrity.[15]

For the target identification related to Type 2 Diabetes Mellitus (T2DM) and liver fibrosis, we conducted a comprehensive search utilizing two well-established databases: OMIM (https://www.omim.org/) and GeneCards (https://www.genecards.org/).[16,17] Initially, for T2DM, we searched the OMIM database using the keyword "Type 2 Diabetes Mellitus" to extract relevant genetic information, including OMIM numbers, gene names, and chromosomal locations. Subsequently, we replicated this process in the GeneCards database, collecting gene-specific information, including GeneCards identifiers, functional annotations, and disease associations. For liver fibrosis, we employed a similar search strategy in both the OMIM and GeneCards databases using the keyword "Liver Fibrosis" ensuring that all pertinent genetic and functional details were recorded. The process allowed us to gather genetic data from OMIM while also obtaining comprehensive biological functions and disease associations

for these genes from GeneCards. After gathering the relevant data, we meticulously organized and deduplicated the target information to ensure the highest level of accuracy and consistency. Finally, we intersected the Curcumin J7 targets with those associated with T2DM and liver fibrosis to identify common targets.

To further investigate the interactions between the identified targets, we utilized the STRING database (https://string-db.org).[18] On the STRING homepage, we selected the "Multiple Proteins" option and entered the names of the common targets, ensuring that each target was entered on a separate line. For species selection, we chose "Homo sapiens" and set the "Minimum required interaction score" to medium confidence (>0.9). We also selected the option to "Hide disconnected nodes in the network." After the search was completed, we downloaded the interaction network data in a suitable format (eg, TSV). This data was then imported into Cytoscape (version 3.9.1) for network visualization, using the File > Import > Network from File menu option. To enhance the analysis, we installed the MCC plugin in Cytoscape and applied the MCC algorithm to rank the nodes in the network. Based on the MCC rankings, we extracted the top six genes for further analysis.

Among the identified genes, we selected the TOP1 genes JUN and RELA as the primary candidates for study. To obtain their three-dimensional structural information, we conducted searches in the Protein Data Bank (PDB) (https://www.rcsb.org/) and successfully downloaded the corresponding PDB format files. Subsequently, we accessed the PubChem database (https://pubchem.ncbi.nlm.nih.gov/) to retrieve two-dimensional structural data for Curcumin J7,[19,20] which served as essential input for the subsequent molecular docking analyses.

Using AutoDockTools-1.5.6 software, we performed molecular docking simulations between the JUN and RELA proteins and the small molecule J7. The docking process aimed to predict the interaction modes and binding affinities between these targets and Curcumin J7. Prior to initiating the docking procedure, we carefully defined critical parameters, including the position and dimensions of the docking box and the resolution of the grid points. Molecular docking simulations were executed using AutoDock Vina and CB-Dock2 (https://cadd.labshare.cn/cb-dock2/php/index.php).[21] Following the docking computations, we obtained multiple binding modes and associated binding free energy values. These results were visually represented using PyMOL software to generate three-dimensional visualizations of the optimal binding modes.

Disease Ontology (DO) Enrichment, Gene Ontology (GO) Enrichment, and KEGG Pathway Enrichment

For the disease enrichment analysis, we selected "Disease Ontology" as the background database and utilized R software to conduct the analysis of the common target genes.[22] We established a significance threshold of p-value < 0.05 to filter for disease categories exhibiting significant enrichment. For each disease category, we calculated the enrichment score and corresponding p-value. The results were then visualized using bar charts, with each disease name and its respective -log10(p-value) color-coded for clarity and ease of interpretation.

Gene Ontology (GO) enrichment analysis was performed to assess three fundamental aspects: Biological Process (BP), Cellular Component (CC), and Molecular Function (MF).[23] The most significantly enriched entries were selected by applying stringent p-value thresholds or other statistical significance criteria. This approach facilitated the identification of key biological processes, cellular components, and molecular functions associated with the common target genes.

Subsequently, we conducted KEGG pathway enrichment analysis on the top six key genes identified from the common targets. A bar graph was generated to represent the number of genes enriched in each pathway, with the -log10 (p-value) visually illustrating the relative significance of the various pathways.[24] This approach provided a comprehensive overview of the biological relevance of the common targets in relation to specific molecular pathways, aiding in the interpretation of their potential therapeutic implications.

Chemical Reagents

The curcumin analog J7, obtained from the School of Pharmacy, Wenzhou Medical University, was dissolved in a 1% sodium carboxymethyl cellulose (CMC-Na) solution for the in vivo experiments. Streptozotocin (STZ) was purchased from Xiamen Xinglongda Chemical Reagent Co., Ltd. (Xiamen, China) and dissolved in citrate buffer for intraperitoneal

injection. STZ is commonly used to induce Type 2 diabetes (T2D) in animal models, as demonstrated in previous studies.[25–28] The high-fat diet used in the study was prepared by the Animal Center of Wenzhou Medical University. The diet comprised 10.0% fat, 20.0% caramel, 2.5% cholesterol, 1.0% bile salt, and 66.5% regular diet components.

Animal Experiments

Sprague Dawley (SD) male rats (n = 60) were adaptively fed with a conventional diet for one week, after which they were randomly divided into a standard control group (NC, n = 10) and an experimental group (n = 50).

The rats in the NC group were continuously fed the conventional diet, while those in the experimental group were fed a high-sugar and high-fat diet for four weeks. Subsequently, the rats in the experimental group were intraperitoneally injected with STZ (35 mg/kg) to induce the development of a type 2 diabetes (T2D) model. Blood glucose levels were measured from the tail vein 72 hours after the injection and again one week later. If the blood glucose level exceeded 16.7 mmol/L, the rat was considered to have a successfully established T2D model. However, eight rats did not meet the blood glucose requirement of 16.7 mmol/L and were therefore excluded from the experiment. As a result, a total of 42 rat models were successfully established in the experimental group.

The rats in the experimental group were further divided into the following groups: diabetes group (Diabetes Mellitus, DM, n = 10), curcumin-treated diabetes group (Curcumin, CUR, n = 12), low-dose curcumin analog J7 treatment group (J7L, n = 10), and high-dose J7 treatment group (J7H, n = 10). The CUR group received a dose of 20 mg/kg/day of curcumin (dissolved in 1% CMC-Na), the J7L group received a dose of 10 mg/kg/day of the curcumin analog J7 (dissolved in 1% CMC-Na), and the J7H group received a dose of 20 mg/kg/day of J7. The doses of curcumin and J7 were selected based on previous studies demonstrating their efficacy and safety in animal models of diabetes and liver fibrosis. Xu et al administered curcumin at 20 mg/kg/day and J7 at 10 mg/kg/day (low dose) and 20 mg/kg/day (high dose), showing that the high dose of J7 exhibited superior antioxidant and anti-fibrotic properties compared to curcumin and the low dose of J7.[29] The rats in all groups were administered the respective treatments via oral gavage for eight weeks.

During the gavage treatment period, eight rats died, including 1 rat in the NC group, 2 rats in the DM group, 3 rats in the CUR group, and 2 rats in the J7H group. The final number of rats included in the experiment was as follows: 9 in the NC group, 8 in the DM group, 7 in the CUR group, 10 in the J7L group, and 8 in the J7H group. After eight weeks of treatment, the rats were euthanized by exsanguination via the femoral vein under deep anesthesia. This method ensures complete blood removal, which is crucial for consistent organ weights and high-quality histological sections, minimizing pooled blood in tissues during dissection.[30] The use of anesthesia prior to exsanguination aligns with the AVMA Guidelines for the Euthanasia of Animals (2020), ensuring that the procedure is humane and causes minimal pain or distress.[31] Throughout the experiment, animal feeding and post-sacrifice procedures strictly adhered to the requirements of the management and protection of experimental animals. The experimental animals were housed in an SPF animal facility with a daily illumination time of 12 hours, a controlled temperature of 18–24°C, approximately 50% humidity, and ad libitum access to water and food.

Analysis of Body Weight and Biochemical Indicators

Throughout the experiment, the rats' weights were measured once a week. Blood samples were collected and allowed to stand at room temperature for 25 minutes. Subsequently, the samples were centrifuged at 1500 g for 20 minutes to separate the serum, which was then stored in a freezer. Fasting blood glucose (FPG), total cholesterol (TC), triglyceride (TG), low-density lipoprotein cholesterol (LDL-c), as well as liver function indices including alanine aminotransferase (ALT) and aspartate aminotransferase (AST), were determined using a Hitachi 7600 biochemical analyzer (Hitachi, Japan).

Microscopic Pathological Analysis

The liver samples obtained from the rats were fixed using paraformaldehyde for histopathological examination with HE staining. Paraformaldehyde is a cross-linking fixative that preserves tissue morphology and cellular structures effectively, making it ideal for general histological studies.[32] For immunohistochemistry (IHC), the tissues were fixed in 10% neutral

buffered formalin, which provides better preservation of antigenicity while maintaining tissue architecture, ensuring accurate detection of target proteins such as NF-κB p65, BAX, and TGF-β1.[33] Additionally, Masson's Trichrome staining was performed to detect collagen deposition. Using an optical microscope (Olympus, Tokyo, Japan), a trained pathologist examined five randomly selected fields of view in all tissue sections under low magnification (40x). These sections were further reviewed by an independent inspector.

Liver fibrosis was assessed and scored on a scale of five severity degrees based on the criteria established by Farrell GC et al: 0 indicated no fibrosis; 1 indicated perisinusoidal hepatic lobule or extracellular fibrosis; 2 indicated periportal fibrosis; 3 indicated lobular zone fibrosis; 4 indicated perisinusoidal fibrosis or bridging fibrosis between portal tracts; and 5 indicated liver cirrhosis.

Electron microscopy, following the protocol by Harmonic G et al, was performed on the liver samples. Briefly, the liver was excised and immersed in liquid nitrogen buffer, fixed in glutaraldehyde at 4°C for 2–4 hours, and subsequently washed, dehydrated, embedded in resin, and sectioned using an ultramicrotome (Leica, Germany). The resulting longitudinal sections were stained with heavy metals (uranyl acetate and lead nitrate) and examined using an H-7500 electron microscope (Hitachi, Tokyo, Japan).

Immunohistochemistry

The formalin-fixed and paraffin-embedded tissues were sectioned to a thickness of 4 mm. Immunohistochemistry was performed following the instructions provided by the manufacturer, and the staining process consisted of two steps. Initially, the sections were blocked using 10% goat serum, after which they were incubated with the appropriate primary antibodies, namely anti-NF-κB p65, anti-BAX-2, or anti-TGF-β1 antibodies (a pilot experiment was conducted to determine the optimal concentration, and a concentration of 1:100, v/v, was found to be most effective). The sections were then incubated overnight at 4°C, followed by incubation with a secondary antibody, such as goat anti-rabbit immunoglobulin G (Santa Cruz, CA, USA). To serve as negative controls for staining, tissue sections incubated with phosphate-buffered saline (PBS) were used in the absence of primary antibodies. To quantify the immunostaining, the Integrated Optical Density (IOD) was measured using Image-Plus 6.0 software. Five randomly selected microscopic fields were analyzed for each sample.

Elisa

The expression levels of NF-κB p65, BAX, BCL-2, IL-1β (interleukin 1 beta), and TGF-β1 in the rats were measured using an enzyme-linked immunosorbent assay (ELISA) kit obtained from Shanghai Bo Yun Biotechnology Co., Ltd. The assay was performed following the instructions provided by the manufacturer. ELISA analyses were performed using serum samples collected independently from at least seven rats per group. No samples were pooled, ensuring all measurements represented independent observations.

While PCR and WB are standard for gene/protein validation, our study prioritized in vivo functional outcomes (eg, fibrosis reduction, metabolic improvements) and ligand-target interaction analyses (via molecular docking) to validate J7's mechanism. These approaches align with recent studies demonstrating that pharmacological interventions in diabetic models can rely on histopathological, biochemical, and docking data to infer target engagement when genetic tools are outside the study's scope.[34,35]

Statistical Analysis

The data obtained from the experiment are presented as mean ± standard deviation. All experimental groups comprised independent biological replicates. Statistical analysis was conducted using GraphPad Prism 5.0 software. To assess the differences between the data sets, a one-way analysis of variance (ANOVA) test was employed. In cases where it was assumed that the data exhibited equal variances, a post hoc Student-Newman-Keuls test was performed to determine significant differences between the groups. Statistical significance was assessed using one-way ANOVA followed by Student-Newman-Keuls post hoc tests. Error bars represent SD to illustrate data variability. Despite apparent overlaps in SD, ANOVA detected significant intergroup differences ($p < 0.05$) due to consistent directional trends and sufficient sample size (n = 7–10 per group). A probability value (P value) of less than 0.05 was considered statistically significant.

Results

Integrating Network Pharmacology and Molecular Docking of Curcumin J7

Figures 1A and B illustrate the identification of a total of 229 curcumin J7 drug targets, 18,795 Type 2 diabetes targets, and 8,400 liver fibrosis targets. The intersection between J7 and Type 2 diabetes yielded 222 common targets, while the overlap between J7 and liver fibrosis identified 201 common targets. These common targets were successfully imported into the STRING database for further analysis and were visualized using Cytoscape.

Employing the MCC (Maximum Clique Centrality) algorithm, the top six key genes associated with the common targets between J7 and Type 2 diabetes were identified: JUN, TP53, STAT3, NFKB1, EP300, and MYC (Figure 1C). In parallel, the top six key genes for the common targets between J7 and liver fibrosis were RELA, NFKB1, IKBKG, IKBKB, CHUK, and TNF (Figure 1D). These genes are likely to play pivotal roles in the underlying biological processes and thus merit further investigation and detailed analysis.

Additionally, after comparing multiple docking conformations, the optimal binding mode was determined by selecting the conformation with the lowest binding free energy. As shown in Figure 1E, the JUN protein exhibited the most favorable binding interaction with Curcumin J7, with a binding free energy of −6.6 kcal/mol. Similarly, Figure 1F demonstrates that the RELA protein exhibited a strong binding affinity for J7, with a binding free energy of −7.2 kcal/mol, indicating a robust binding interaction between the two.

Enrichment Analysis of Common Targets

Between J7 and Type 2 Diabetes

Figure 1G presents the disease enrichment analysis of common targets shared between J7 and Type 2 diabetes. The results highlight six key diseases that exhibit significant enrichment: metabolic dysfunction-associated fatty liver disease, alcoholic hepatitis, hepatobiliary diseases, liver diseases, fatty liver disease, and metabolic dysfunction-associated steatohepatitis. These findings suggest that these diseases may share critical molecular mechanisms or pathways with both J7 and Type 2 diabetes, indicating potential therapeutic intersections.

Figure 1H illustrates the results of the Gene Ontology (GO) enrichment analysis. In the context of biological processes (BP), a notable enrichment was observed in the regulation of carbohydrate metabolic processes, with a particular emphasis on the catabolic process of carbohydrates—a pathway closely linked to the pathological mechanisms of Type 2 diabetes. Furthermore, genes were significantly enriched in processes such as positive regulation of miRNA transcription, the transforming growth factor beta receptor signaling pathway, and regulation of transcription initiation from the DNA template. These findings underscore the potential roles of gene expression regulation and cell signaling in the pathogenesis of diabetes.

The cellular component (CC) enrichment analysis revealed that these genes are predominantly associated with the RNA polymerase II transcriptional regulator complex, the histone acetyltransferase complex, DNA damage sites, the perinuclear region, and the transcriptional repressor complex. These associations suggest that the genes may influence gene expression through the formation of transcription-related complexes within the cell nucleus, providing insight into the molecular mechanisms underlying J7's action. In terms of molecular function (MF), the enrichment analysis identified key functions including NF-κB binding, ligand-activated transcription factor activity, histone acetyltransferase activity, tau protein binding, and transcription coactivator binding. These findings emphasize the significant role of these genes in regulating gene expression, particularly through transcriptional coactivation and transcription factor activity. Notably, the enrichment of enzyme activity further suggests that these genes may play a direct role in metabolic pathways, aligning with the metabolic disturbances observed in Type 2 diabetes.

The KEGG pathway enrichment analysis (Figure 1I) revealed that the key pathways associated with the common targets primarily encompass viral infection, signal transduction, diabetic complications, apoptosis, and cancer—all of which are highly relevant to the biological functions of J7 and its role in the pathological processes of Type 2 diabetes. Specifically, the significantly enriched pathways include Hepatitis B, Kaposi sarcoma-associated herpesvirus infection, Epstein-Barr virus infection, Viral carcinogenesis, Human T-cell leukemia virus 1 infection, Wnt signaling pathway, and lipid and atherosclerosis. The enrichment of these pathways suggests that J7 may influence viral infection pathways and

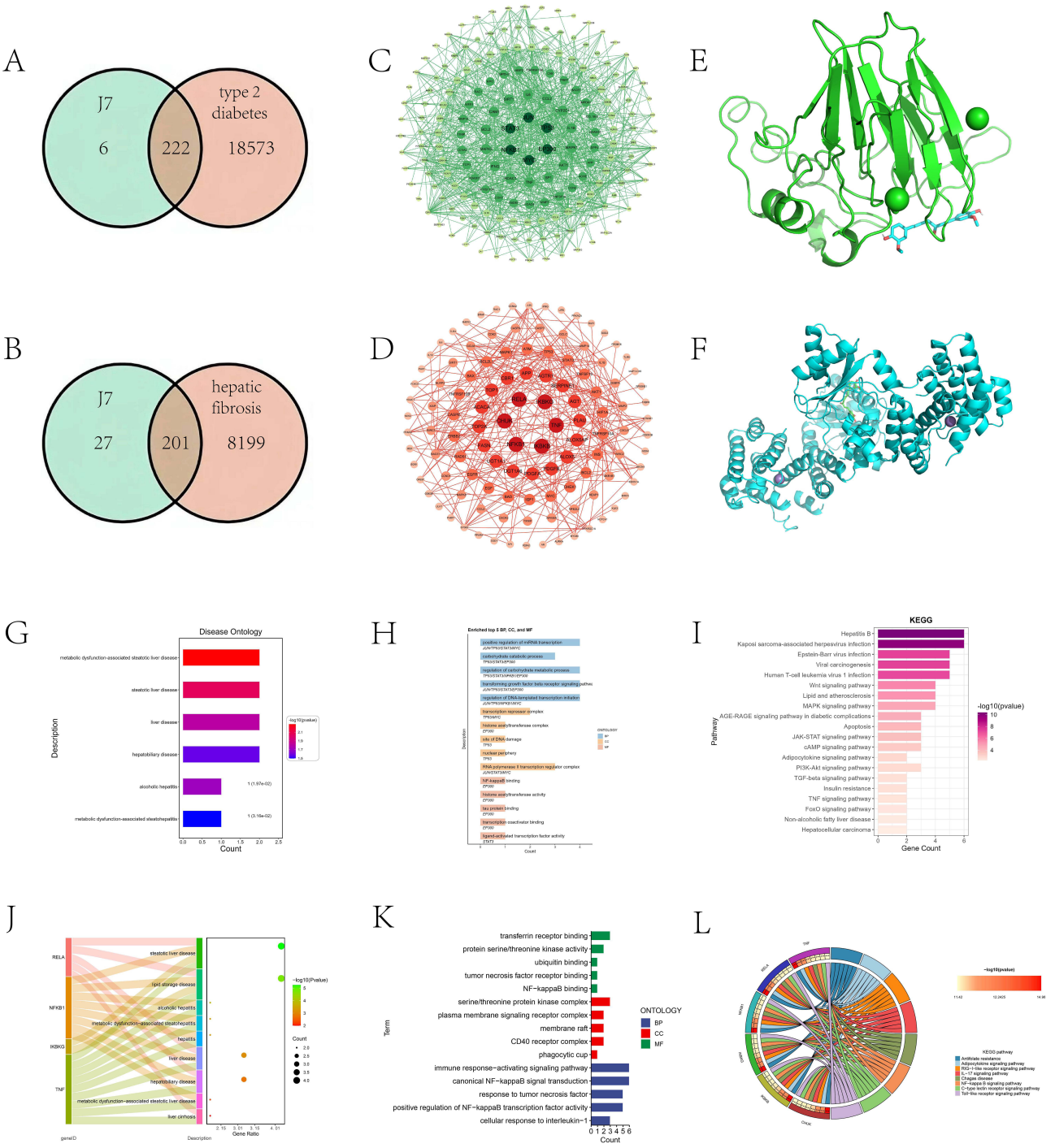

Figure 1 Analysis of J7's Impact on Type 2 Diabetes and Liver Fibrosis. **(A)** Identification of 229 J7 targets, with 222 and 201 common targets for type 2 diabetes and liver fibrosis, respectively.**B)** Common targets for type 2 diabetes and liver fibrosis. **(C)** Top 6 key genes for J7's interaction with type 2 diabetes: JUN, TP53, STAT3, NFKB1, EP300, MYC. **(D)** Top 6 key genes for J7's interaction with liver fibrosis: RELA, NFKB1, IKBKG, IKBKB, CHUK, TNF. **(E)** Optimal binding energy between J7 and JUN (−6.6 kcal/mol). **(F)** Optimal binding energy between J7 and RELA (−7.2 kcal/mol). **(G)** Disease and pathway enrichment analysis for J7 and type 2 diabetes common targets. **(H)** Pathway enrichment analysis for J7 and type 2 diabetes. **(I)** Disease enrichment analysis for J7 and type 2 diabetes. **(J)** Disease and pathway enrichment analysis for J7 and liver fibrosis common targets, highlighting roles in immune response and inflammation. **(K)** Pathway enrichment analysis for J7 and liver fibrosis. **(L)** Disease enrichment analysis for J7 and liver fibrosis.

Abbreviations: **J7**, curcumin analog J7; **JUN**, Jun proto-oncogene; **TP53**, Tumor protein p53; **STAT3**, Signal transducer and activator of transcription 3; **NFKB1**, Nuclear factor kappa B subunit 1; **EP300**, E1A binding protein p300; **MYC**, Myc proto-oncogene protein; **RELA**, V-rel avian reticuloendotheliosis viral oncogene homolog A; **IKBKG**, Inhibitor of nuclear factor kappa B kinase gamma; **IKBKB**, Inhibitor of nuclear factor kappa B kinase beta; **CHUK**, Cellular helical unit kinase; **TNF**, Tumor necrosis factor.

https://doi.org/10.2147/DDDT.S511372

signal transduction processes, potentially contributing to the onset and progression of Type 2 diabetes. The significant enrichment of virus-related pathways, such as Hepatitis B and Kaposi sarcoma-associated herpesvirus infection, points to the potential role of viral infections in the pathophysiology of diabetes.

Furthermore, the activation of signaling pathways such as the Wnt signaling pathway, MAPK signaling pathway, and AGE-RAGE signaling pathway in the context of diabetic complications indicates a strong association with key characteristics of Type 2 diabetes, including insulin resistance and dysregulated cell metabolism. These findings underscore J7's potential involvement in regulating these critical pathways. Notably, the enrichment analysis also highlighted pathways directly related to diabetes and its complications, such as apoptosis, insulin resistance, non-alcoholic fatty liver disease (NAFLD), and hepatocellular carcinoma. These insights not only provide a novel perspective on the molecular connections between J7 and Type 2 diabetes but also establish an important theoretical foundation for further research into prevention and treatment strategies targeting both diabetes and its associated complications.

Between J7 and Liver Fibrosis

Through disease enrichment analysis of the top six key genes associated with the common targets of J7 and liver fibrosis, we identified that these genes play a pivotal role in various liver diseases, closely correlating with the pathological mechanisms underlying both J7's therapeutic effects and liver fibrosis. Figure 1J illustrates that these key genes exhibit significant alterations in expression levels or functional activities in diseases such as non-alcoholic fatty liver disease (NAFLD), steatotic liver disease, alcoholic hepatitis, metabolic dysfunction-associated steatohepatitis (MDASH), hepatitis, and liver cirrhosis. Specifically, the elevated expression of these genes in NAFLD suggests that J7 may be involved in hepatocyte steatosis, while its expression alterations in alcoholic hepatitis and common hepatitis indicate a potential role for J7 in modulating the liver's inflammatory response. Furthermore, the expression patterns observed in liver cirrhosis provide insights into J7's involvement in the progression of liver fibrosis, possibly through mechanisms such as liver cell damage repair and collagen deposition. These findings not only enhance our understanding of J7's potential in liver diseases but also introduce new targets and a theoretical foundation for devising therapeutic strategies for liver diseases like fibrosis.

Figure 1K presents the results of Gene Ontology (GO) enrichment analysis for the top six key genes associated with the common targets between J7 and liver fibrosis. In the context of biological processes (BP), these genes are notably enriched in processes such as the activation of immune response signaling pathways, positive regulation of NF-κB transcription factor activity, classical NF-κB signaling, response to tumor necrosis factor, and cellular response to interleukin-1. These enrichment results underscore the crucial role of these genes in modulating immune responses and inflammatory reactions, which are intimately tied to the pathological mechanisms of both J7 and liver fibrosis. In particular, the involvement of these genes in the NF-κB signaling pathway may exacerbate inflammation and liver cell damage, thereby facilitating the progression of liver fibrosis.

In terms of cellular components (CC), the analysis reveals significant enrichment in cellular structures such as the CD40 receptor complex, serine/threonine protein kinase complex, membrane rafts, plasma membrane signaling receptor complex, and phagocytic cups. These structures are key to immune and inflammatory signaling, suggesting that the genes are critical for cell membrane-related signaling and phagocytic activities, both of which contribute to the pathophysiology of liver fibrosis.

The molecular function (MF) enrichment analysis highlights several vital roles for these genes, including transferrin receptor binding, protein serine/threonine kinase activity, NF-κB binding, tumor necrosis factor receptor binding, and ubiquitin binding. These functions are integral to cell signaling, protein modification, and inflammatory responses, further emphasizing the significance of these genes in the pathological processes associated with J7 and liver fibrosis. For example, tumor necrosis factor receptor binding likely contributes to inflammation-driven liver cell damage, while ubiquitin binding may play a role in the degradation of damaged liver cell proteins and the maintenance of intracellular homeostasis.

Figure 1L illustrates the KEGG pathway enrichment analysis for the key targets through which J7 exerts its effects in liver fibrosis. The enriched pathways include Antifolate resistance, Adipocytokine signaling pathway, RIG-I-like receptor signaling pathway, IL-17 signaling pathway, Chagas disease, and NF-κB signaling pathway. Notably, the Antifolate

resistance and Adipocytokine signaling pathway pathways are of particular significance in the development of liver fibrosis, suggesting that J7 may exert its antifibrotic effects by modulating these pathways. Furthermore, the enrichment of the RIG-I-like receptor and IL-17 signaling pathways indicates that J7 may mitigate the progression of liver fibrosis by influencing immune responses and inflammatory reactions. The activation of the NF-κB signaling pathway, a key factor in liver fibrosis progression, also highlights J7's potential role in regulating this pathway, providing further insight into its antifibrotic mechanisms.

General Conditions of Rats

During the establishment of the diabetes model, rats in the DM group exhibited symptoms of polydipsia (increased thirst), polyphagia (increased appetite), and diuresis (excessive urination). In contrast, the food and water intake of rats in the other groups remained normal and healthy. Unfortunately, the model establishment was unsuccessful in 8 rats within the DM group, leading to their exclusion from the experiment. Additionally, there were some cases of rat mortality during the feeding process, with 1 rat in the NC group, 2 rats in the DM group, 3 rats in the CUR group, and 2 rats in the J7H group being affected.

The mortality in the NC group may be attributed to natural causes or stress associated with handling and gavage procedures, as this group was not subjected to diabetes induction or high-fat diet feeding. In the diabetic groups (DM, CUR, J7L, J7H), mortality could be linked to the severe metabolic dysregulation and complications associated with type 2 diabetes, such as hyperglycemia, oxidative stress, and organ damage. The higher mortality in the CUR and J7H groups may reflect the challenges of managing advanced diabetic complications, despite the therapeutic interventions. These findings are consistent with previous studies reporting similar mortality rates in diabetic animal models due to the progressive nature of the disease and its complications.[36] All procedures were conducted in compliance with ethical guidelines, and efforts were made to minimize stress and discomfort to the animals.

Comparison of Body Weight

During the initial grouping, there were no significant differences in the weights of rats among the various groups. However, after four weeks of being fed a high-glucose and high-fat diet, the body weight of the rats in the NC group naturally increased, while the body weight of the experimental groups showed a decrease. The body weights of the rats in each group after the 8-week experiment are depicted in Figure 2A and B (Please refer to supplementary figure 2).

Statistical analysis revealed that the body weight of the DM group was significantly lower than that of the NC group ($P < 0.05$), indicating a significant difference between the two groups. Conversely, the body weights of the rats in the CUR group, J7L group, and J7H group showed an increase.

Blood Biochemical Status in Rats

Fasting Blood Glucose and Blood Lipid Test Results

The serum fasting blood glucose (FPG), triglyceride (TG), total cholesterol (TC), and low-density lipoprotein (LDL) levels in the DM group were found to be significantly higher compared to those in the NC group ($P < 0.05$). However, in the CUR, J7L, and J7H groups, the FPG, TG, TC, and LDL levels were significantly decreased when compared to the DM group ($P < 0.05$). These findings indicate that the administration of the curcumin analog J7 can effectively reduce blood glucose and blood lipid levels to a certain extent, as demonstrated in Figure 2A–G (Please refer to supplementary figure 2).

Results of Serum Liver Function Test

The serum levels of alanine aminotransferase (ALT) and aspartate aminotransferase (AST) in the DM group were found to be higher compared to those in the NC group ($P < 0.05$). However, after the administration of curcumin and J7 treatment, the ALT and AST levels in the CUR, J7L, and J7H groups exhibited a significant decrease ($P < 0.05$). These findings suggest that the curcumin analog J7 has the ability to treat liver injury induced by diabetes, and it shows comparable efficacy to traditional curcumin. Moreover, the efficacy of curcumin analog J7 was found to be independent of the dosage used, as shown in Figure 2H and I (Please refer to supplementary figure 2).

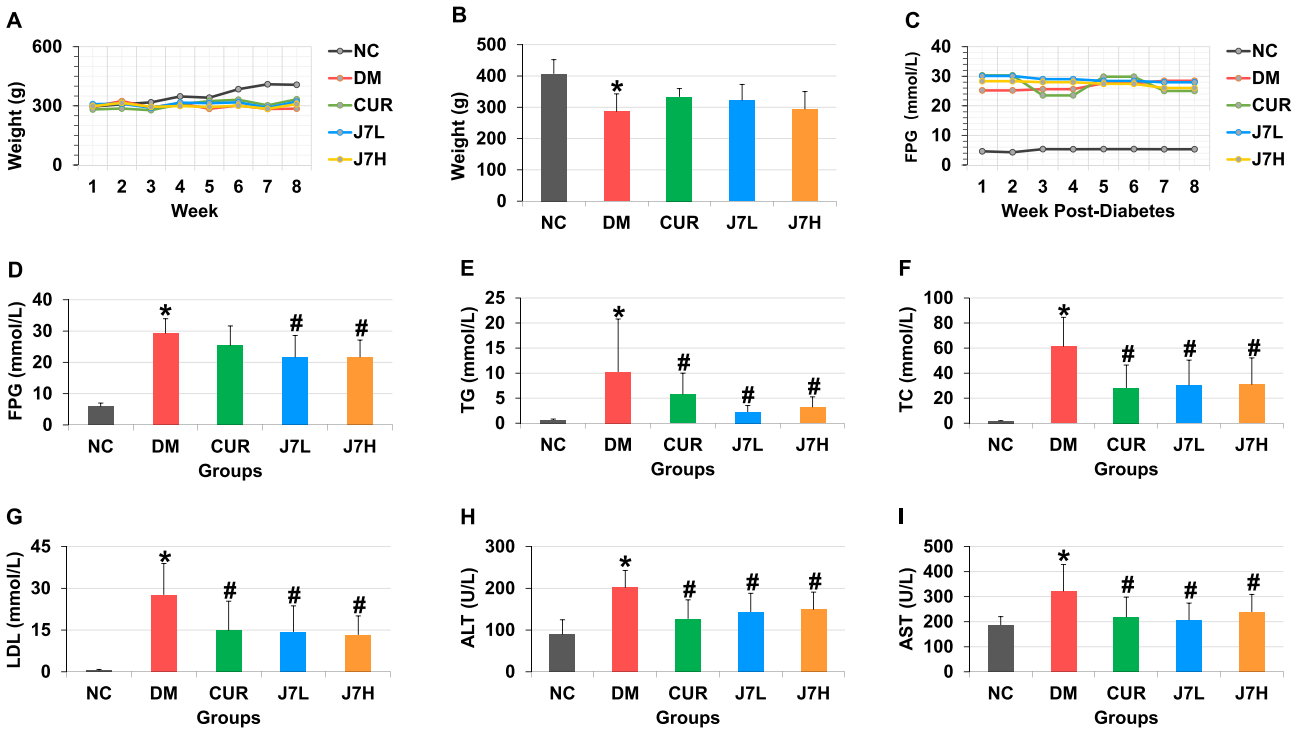

Figure 2 Changes in body weight and biochemical analysis of SD rats in NC, DM, CUR, J7L, and J7H groups. **(A)** Average body weight of SD rats in all groups over 8 weeks. **(B)** Individual body weights of SD rats. **(C)** Average fasting plasma glucose (FPG) levels in all groups after 8 weeks of diabetes induction. **(D)** FPG levels. **(E)** Triglyceride (TG) levels. **(F)** Total cholesterol (TC) levels. **(G)** Low-density lipoprotein (LDL) levels. **(H)** Alanine aminotransferase (ALT) levels. **(I)** Aspartate aminotransferase (AST) levels.
Abbreviations: SD, Sprague Dawley; **NC**, normal control group; **DM**, diabetes group; **CUR**, curcumin treatment group; **J7L**, curcumin analog J7 low-dose treatment group; **J7H**, curcumin analog J7 high-dose treatment group; **FPG**, fasting plasma glucose; **TG**, triglyceride; **TC**, total cholesterol; **LDL**, low-density lipoprotein; **ALT**, alanine aminotransferase; **AST**, aspartate aminotransferase. All data in Figure 8B and 8D–**I** are presented as **Mean ± Standard Deviation. *P < 0.05 vs NC; #P < 0.05 vs DM**.

Morphological Observation of Liver

HE Staining Observation

Figure 3A illustrates the liver lobule, where hepatocytes are cuboidal in shape and arranged in a regular pattern. In the DM group, multifocal inflammatory cell infiltration into the hepatocytes was observed. Additionally, cell damage, including water degeneration, balloon-like degeneration, and steatosis, was evident. However, following treatment with curcumin, J7L, and J7H, the liver degeneration in the CUR, J7L, and J7H groups showed alleviation.

Masson Staining Observation

In comparison to the NC group, the liver structure in the DM group exhibited similarities to that of obesity. Numerous fat droplets of varying sizes were diffusely distributed throughout the cytoplasm. Infiltration of inflammatory cells, such as lymphocytes, monocytes, and plasma cells, was observed. In Masson staining, the degree of collagen fiber hyperplasia and fibrosis was graded. The grading of liver fibrosis is presented in Figure 3B (Please refer to supplementary figure 2). The livers of DM rats showed further damage with multifocal inflammatory cell infiltration and evident steatosis, which disrupted the normal hepatic cords.

Furthermore, there was an abundance of collagen fibers, even in the portal vein area, and the diaphragm exhibited increased thickness and fibrosis. After treatment, fibrosis was alleviated as indicated by a reduction in the area of bright green matrix observed in Masson staining. Curcumin and J7 treatments resulted in a decrease in the number of collagen fibers, with the J7H group showing a more pronounced reduction. These data demonstrate that curcumin and J7 have the potential to treat liver fibrosis and protect the liver, as shown in Figure 3A. The Masson classification for liver fibrosis is presented in Figure 3B.

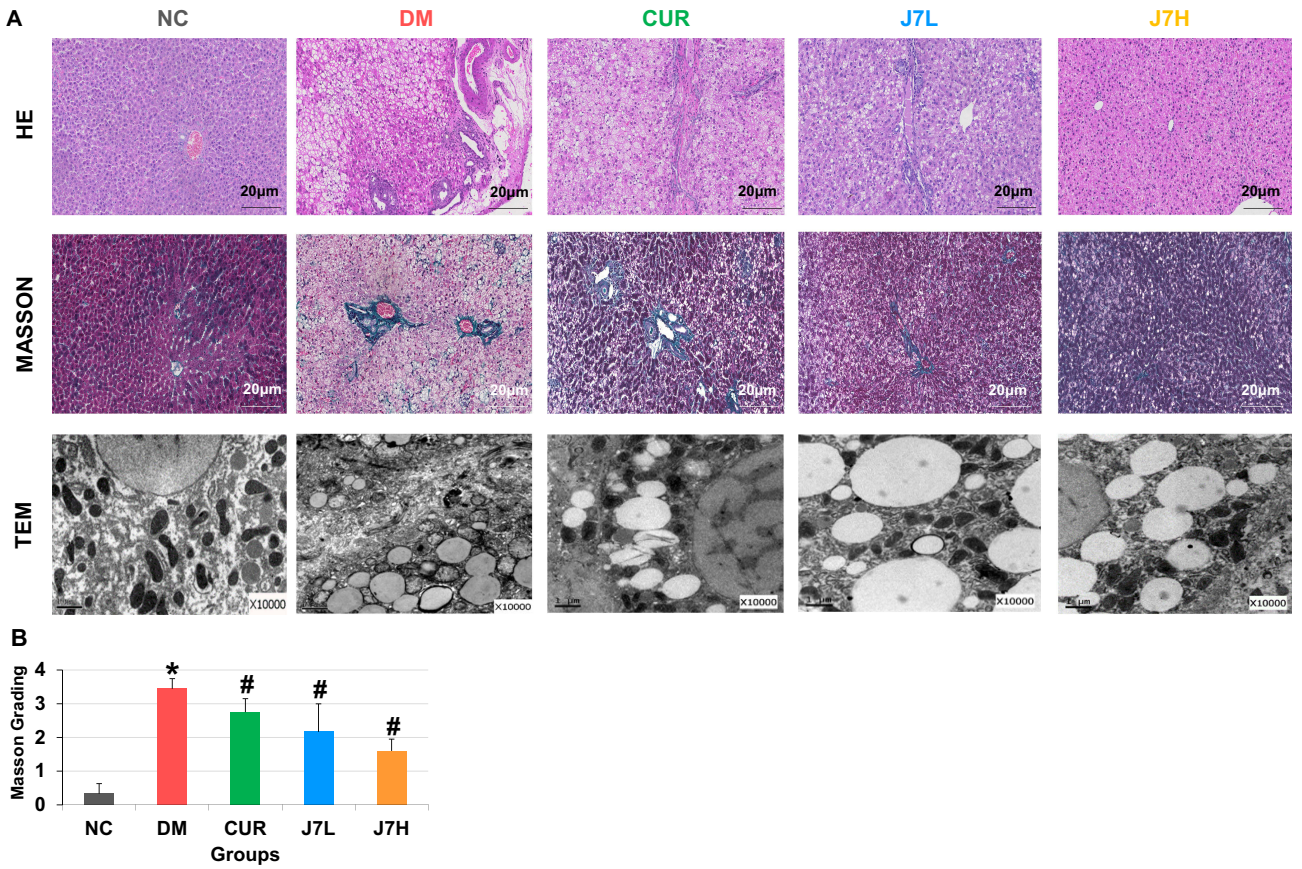

Figure 3 Pathological changes in the liver of diabetic rats before and after treatment. **(A)** Panels include hematoxylin and eosin (HE) staining (scale bar: 20 μm), Masson staining (scale bar: 20 μm), and ultrastructure visualization under transmission electron microscopy (TEM) (scale bar: 1 μm). HE staining revealed liver inflammation in the DM group, which was alleviated in CUR- and J7-treated rats. Masson staining showed collagen fiber proliferation in the DM group, which was reduced following CUR and J7 treatment. TEM analysis demonstrated that lipid particles in the DM group fused into giant fat droplets, whereas lipid accumulation was reduced in CUR- and J7-treated rats. **(B)** Liver fibrosis grading in SD rats. **Abbreviations: HE**, hematoxylin and eosin; **TEM**, transmission electron microscopy; **NC**, normal control group; **DM**, diabetes group; **CUR**, curcumin treatment group; **J7L**, curcumin analog J7 low-dose treatment group; **J7H**, curcumin analog J7 high-dose treatment group; **SD**, Sprague Dawley. All data in Figure 3B are presented as **Mean ± Standard Deviation. *P < 0.05 vs NC; #P < 0.05 vs DM**.

Observation Results of the Liver by Electron Microscope

Upon electron microscopic observation, the liver nucleus in the NC group appeared oval, with a clear and unswollen hepatic nuclear structure. The mitochondria were oval in shape, rich in crista, and exhibited intact mitochondrial membranes. Furthermore, the mitochondria were arranged in a regular manner. In the DM liver, there was an increased number of lipid particles, with some particles merging to form large lipid droplets of varying sizes. These lipid particles were distributed throughout the cytoplasm. Additionally, the DM liver exhibited an increased number of rough endoplasmic reticulum, fusion of karyotypes, deepening of chromatin, and mitochondrial swelling. The density of mitochondria was also increased, and their crista exhibited a disorganized arrangement. Disappearance and disruption of mitochondrial crista, as well as collagen fibrosis, were observed in the DM liver.

In contrast, in the CUR, J7L, and J7H groups, the number of lipid particles in rat liver cells was reduced, and nuclear deflation was minimized. Furthermore, there was an increased number of mitochondria, and the swelling of mitochondria was significantly reduced (as depicted in Figure 3C).

Immunohistochemistry: The Expression of TGF-β1, NF-κBp65, and BAX in Liver Tissue

In the NC group, the expression of TGF-β1 in liver tissue was minimal. However, compared to the NC group, the expression of TGF-β1 in the cytoplasm of hepatic cells near the portal vein and central vein was significantly increased in the DM group. Following intervention with curcumin and its analog J7, the expression of TGF-β1 in the CUR, J7L, and J7H groups was significantly reduced (as shown in Figure 4A – C) (Please refer to supplementary figure 2).

https://doi.org/10.2147/DDDT.S511372

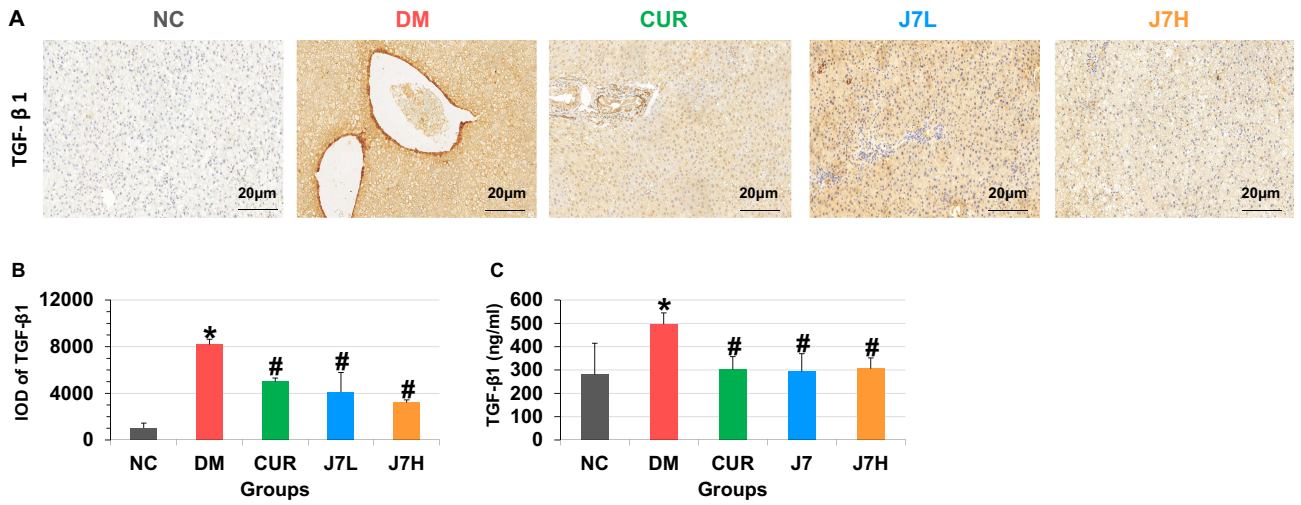

Figure 4 Immunohistochemical (IHC) staining and TGF-β1 expression in the liver of SD diabetic rats before and after treatment. **(A)** Immunohistochemical staining of TGF-β1 in liver tissue (scale bar: 20 μm). **(B)** Integrated optical density (IOD) analysis of TGF-β1 expression. **(C)** Expression level of TGF-β1. TGF-β1 expression was significantly increased in the liver tissue of the DM group, while CUR and J7 treatment reduced its expression.
Abbreviations: IHC, immunohistochemistry; **TGF-β1**, transforming growth factor β1; **SD**, Sprague Dawley; **IOD**, integrated optical density; **NC**, normal control group; **DM**, diabetes group; **CUR**, curcumin treatment group; **J7L**, curcumin analog J7 low-dose treatment group; **J7H**, curcumin analog J7 high-dose treatment group; **GAPDH**, glyceraldehyde 3-phosphate dehydrogenase. All data in Figure 4B and C are presented as **Mean ± Standard Deviation. *P < 0.05 vs NC; #P < 0.05 vs DM**.

Similarly, the NC group exhibited almost no positive expression of NF-κB p65. However, in the DM group, the expression of NF-κB p65 was significantly enhanced. In contrast, the positive expression of NF-κB p65 in the CUR, J7L, and J7H groups was significantly lower compared to the DM group. These results indicate that curcumin and its analog J7 have the ability to inhibit the expression of NF-κB p65 in diabetic rats (as depicted in Figure 5A – C) (Please refer to supplementary figure 2).

Regarding the expression of BAX, it was significantly lower in the hepatocytes of the DM group compared to the NC group. The expression of BAX in the DM group was primarily observed in the hepatocyte cytoplasm. After treatment with curcumin and its analog J7, the expression of BAX was significantly reduced, suggesting that curcumin and its analog J7 can inhibit BAX expression in the liver of diabetic rats, thereby inhibiting hepatocyte apoptosis and protecting the liver (as shown in Figure 6A – C) (Please refer to supplementary figure 2).

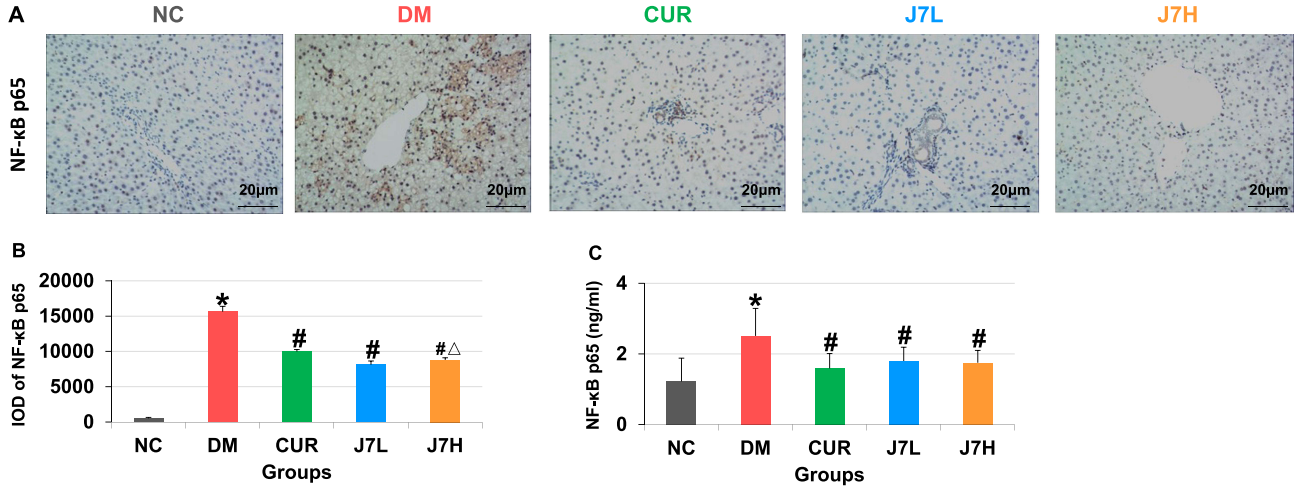

Figure 5 IHC staining and NF-κB p65 ELISA in the liver of SD diabetic rats before and after treatment. **(A)** Immunohistochemical (IHC) staining of NF-κB p65 in liver tissue (scale bar: 20 μm). **(B)** Integrated optical density (IOD) analysis of NF-κB p65 expression. **(C)** NF-κB p65 expression levels. NF-κB p65 expression was significantly increased in the liver tissue of the DM group, while CUR and J7 treatment significantly reduced its expression.
Abbreviations: IHC, immunohistochemistry; **NF-κB p65**, nuclear factor kappa-light-chain-enhancer of activated B cells p65; **SD**, Sprague Dawley; **IOD**, integrated optical density; **NC**, normal control group; **DM**, diabetes group; **CUR**, curcumin treatment group; **J7L**, curcumin analog J7 low-dose treatment group; **J7H**, curcumin analog J7 high-dose treatment group. All data in Figures 5B and C are presented as **Mean ± Standard Deviation. *P < 0.05 vs NC; #P < 0.05 vs DM; ΔP <0.05 relative to CUR**.

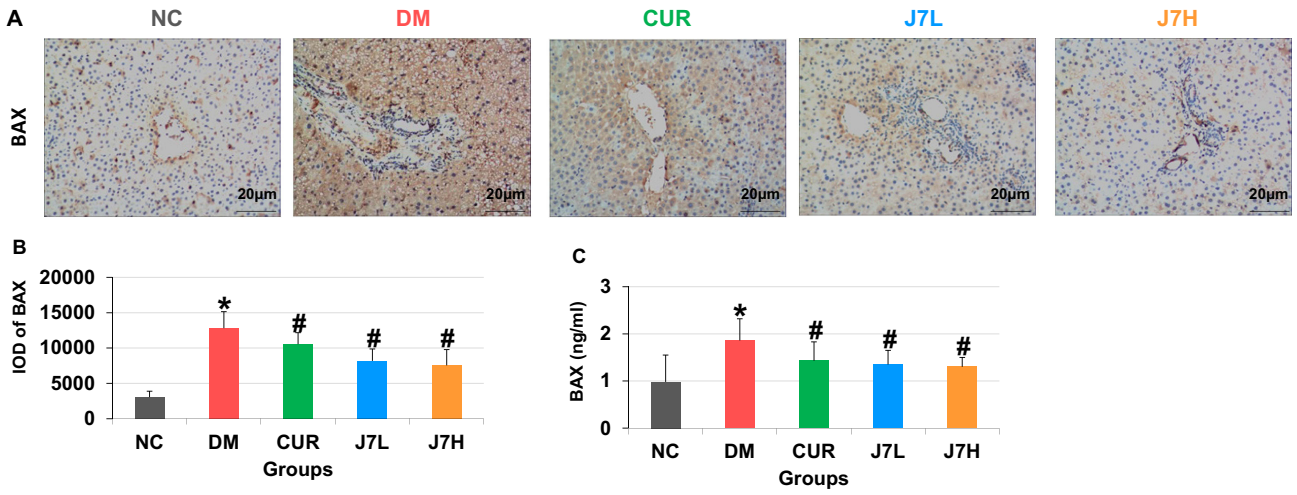

Figure 6 IHC staining and BAX ELISA in the liver of SD diabetic rats before and after treatment. **(A)** Immunohistochemical (IHC) staining of BAX in liver tissue (scale bar: 20 μm). **(B)** Integrated optical density (IOD) analysis of BAX expression. **(C)** BAX expression levels. BAX expression was significantly increased in the liver tissue of the DM group, while CUR and J7 treatment reduced its expression.

Abbreviations: IHC, immunohistochemistry; **BAX**, BCL2-associated X protein; **SD**, Sprague Dawley; **IOD**, integrated optical density; **NC**, normal control group; **DM**, diabetes group; **CUR**, curcumin treatment group; **J7L**, curcumin analog J7 low-dose treatment group; **J7H**, curcumin analog J7 high-dose treatment group. All data in Figures 6B and C are presented as **Mean ± Standard Deviation. *P < 0.05 vs NC; #P < 0.05 vs DM**.

ELISA Determination: Measurement Results of NF-κB p65, IL-1β, TGF-β1, BAX, BCL-2, BCL-2 / BAX, and Caspase 3

In this study, we quantitatively examined the expression levels of important inflammatory factors and proteins connected to apoptosis in the supernatants of different cell cultures using the enzyme-linked immunosorbent assay (ELISA) (Please refer to supplementary figure 2). The results of the experiment showed that the diabetic model group (DM) had a significantly higher level of interleukin-1β (IL-1β) than the negative control group (NC) (Figure 7A), suggesting that the inflammatory response is triggered under diabetes settings.

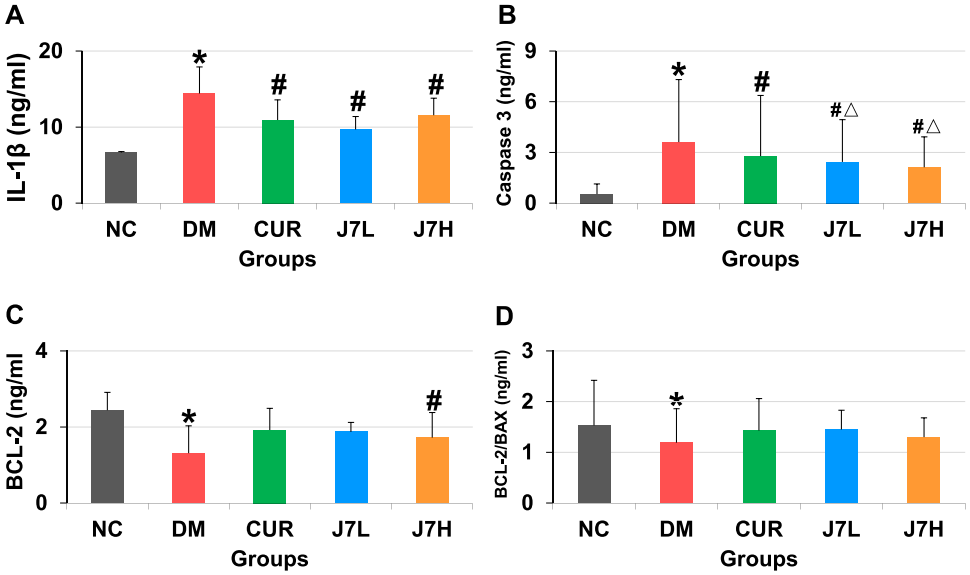

Figure 7 Expression levels in the liver of SD diabetic rats before and after treatment. **(A)** Expression levels of IL-1β. **(B)** Expression levels of BCL-2. **(C)** BCL-2/BAX expression ratio. **(D)** Expression levels of caspase-3.

Abbreviations: **SD**, Sprague Dawley; **NC**, normal control group; **DM**, diabetes group; **CUR**, curcumin treatment group; **J7L**, curcumin analog J7 low-dose treatment group; **J7H**, curcumin analog J7 high-dose treatment group; **IL-1β**, interleukin-1 beta; **BCL-2**, B-cell lymphoma 2; **BAX**, BCL2-associated X protein. All data are presented as **Mean ± Standard Deviation. *P < 0.05 vs NC; #P < 0.05 vs DM; ΔP <0.05 relative to CUR**.

https://doi.org/10.2147/DDDT.S511372

The abnormal activation of the apoptosis pathway in the diabetic state was revealed by the concurrent significant increase in the level of the pro-apoptotic protein caspase-3 (Figure 7B) and significant decrease in the DM group of the anti-apoptotic protein B-cell lymphoma-2 (BCL-2) (Figure 7C). Notably, we discovered that curcumin (CUR) considerably undid these alterations following therapy, with the group treated with CUR showing a much lower level of IL-1β than the DM group (Figure 7A), indicating a considerable anti-inflammatory impact of CUR.

These findings give strong experimental support for the prospective use of CUR in the treatment of diabetes and its complications, as well as confirming the possible involvement of CUR in controlling the production of proteins related to inflammation and apoptosis. In addition, we examined the Bcl-2/Bax ratio, which is a crucial sign of the apoptotic tendency. The findings indicated that while the Bcl-2/Bax ratio in the CUR group remained lower than in the NC group, it exhibited improvement in comparison to the DM group (Figure 7D), suggesting that the treatment may help lessen the tendency toward apoptosis brought on by diabetes.

The results of our study also demonstrated that the effects of CUR treatment were greater than those of the positive control drug J7H in lowering IL-1β and caspase-3 levels and raising BCL-2 expression. In conclusion, our ELISA data demonstrate the dysregulation of the apoptotic and inflammatory pathways in the diabetic state and offer scientific support for CUR as a successful treatment approach, which may be directly linked to the control of these important proteins. The subsequent research studies will delve deeper into the precise mechanisms of action of CUR and establish the groundwork for its clinical implementation.

Docking Results

The docking simulation technique is a convenient and effective method for investigating the interaction between small molecules and target proteins. Here, we used the Vina 1.2.3 software to study the docking of compound J7 with BCL-2 and BAX proteins. Based on the docking results of J7 with BAX, the left image provides an overall view, while the right image offers a detailed view. In the figures, the yellow sticks represent the small molecule, the cyan cartoons represent the protein, blue lines indicate hydrogen bonding, grey dashed lines indicate hydrophobic interactions, and orange dashed lines represent cation-pi interactions (Figure 8A).

As shown in Figure 8B, the interaction map of small molecule J7 with the BAX protein reveals that J7 forms hydrogen bonds with ARG-89 and cation-pi interactions with ARG-94. The formation of hydrogen bonds and salt bridges leads to a tighter binding between the protein and the small molecule. Additionally, hydrophobic interactions with ARG-89, ARG-94, ALA-139, ASP-142, and PHE-93 provide significant van der Waals forces for the molecule.

Regarding the binding mode of J7 with BCL-2, the left image shows the overall view, and the right image shows the local view. In the figures, the yellow sticks represent the small molecule, the cyan cartoons represent the protein, blue lines indicate hydrogen bonding, grey dashed lines indicate hydrophobic interactions, and magenta dashed lines represent pi-pi interactions (Figure 8B and C).

As depicted in Figure 8C, the interaction map of small molecule J7 with the BCL-2 protein shows that J7 engages in pi-pi interactions with TYR-202. It also forms hydrophobic interactions with TYR-108, ALA-100, ALA-149, PHE-104, and ARG-146, providing strong van der Waals forces for the molecule.

A negative binding affinity score indicates the possibility of binding, with lower values generally suggesting a higher likelihood of binding. In this complex, the docking software provided binding affinity scores of −7.416 and −7.617 kcal/mol for J7 with BCL-2 and BAX, respectively, indicating a favorable binding of J7 to both BCL-2 and BAX proteins (Please refer to supplementary figure 1).

Discussion

The rapid evolution of medical science has heralded a new era in which network pharmacology plays a pivotal role in predicting drug mechanisms.[37] By seamlessly integrating principles and techniques from diverse disciplines—such as biology, pharmacology, bioinformatics, and network science—network pharmacology has significantly advanced drug discovery and the elucidation of complex disease mechanisms.

Notably, the pioneering contributions of Andrew L. Hopkins and his et.al were instrumental in establishing the theoretical underpinnings of network pharmacology, thereby highlighting its critical role in deciphering biological

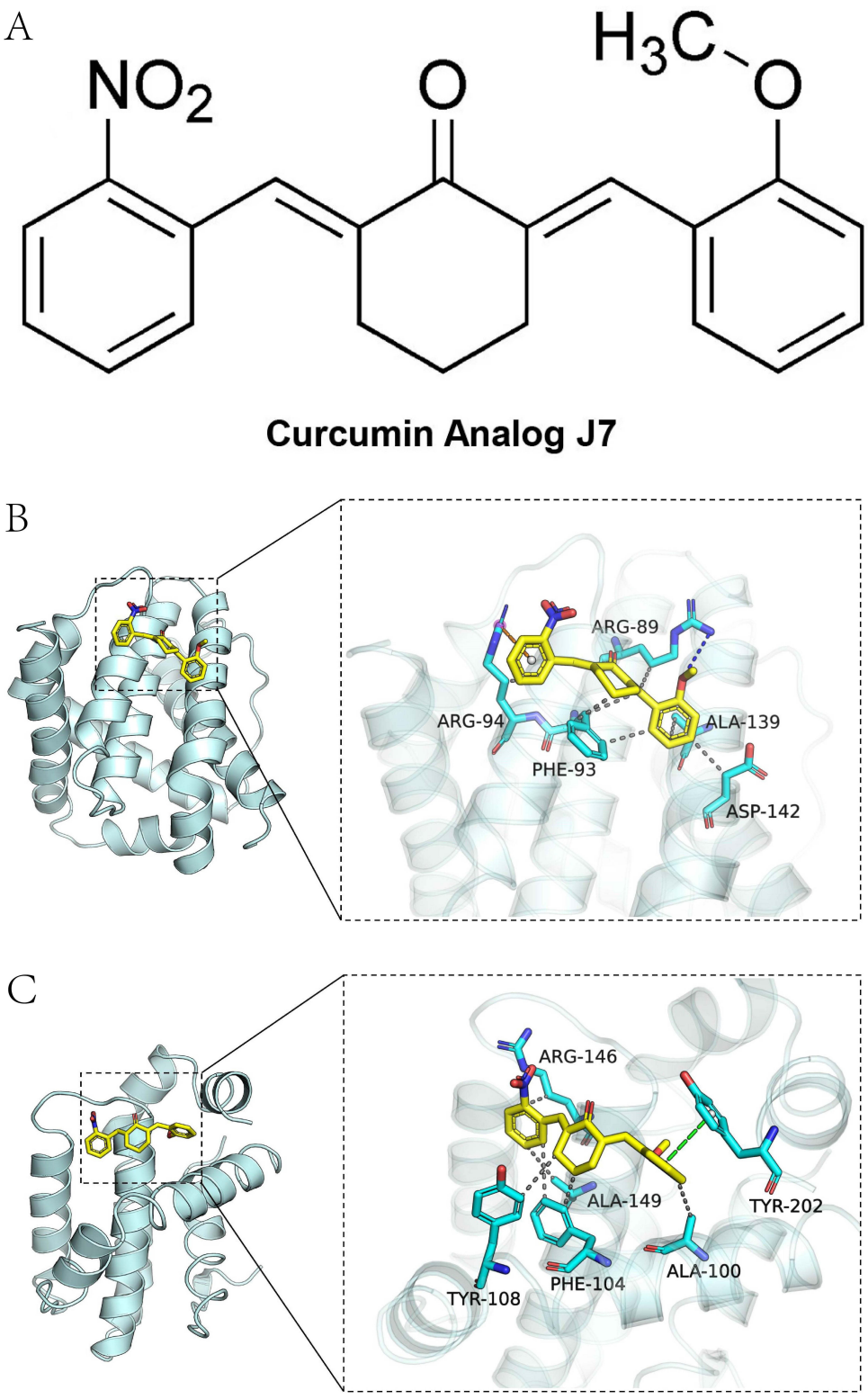

Figure 8 Molecular docking results. **(A)** Chemical structure of the curcumin analog J7. **(B)** Docking complex of BAX and J7, showing the binding interactions. **(C)** Docking complex of BCL2 and J7, illustrating the molecular interactions.
Abbreviations: BAX, BCL2-associated X protein; **BCL2**, B-cell lymphoma 2.

https://doi.org/10.2147/DDDT.S511372

systems.[38] Building on this foundational work, subsequent investigations have refined the discipline by integrating advanced enrichment analysis methodologies.

Enrichment analysis, an indispensable tool in bioinformatics, enables the systematic identification of critical biological pathways and molecular interactions. In the present study, we utilize three well-established methods—Gene Ontology (GO) enrichment analysis, Kyoto Encyclopedia of Genes and Genomes (KEGG) pathway enrichment analysis, and Disease Ontology enrichment analysis—to delineate drug action pathways and clarify disease pathogenesis. Collectively, these approaches provide a robust theoretical framework that underpins experimental investigations, drug development, and clinical applications.[39]

In parallel, the integration of molecular docking techniques has become increasingly prevalent in network pharmacology, further refining our understanding of drug–disease interactions.[40] Originally developed as a computer-aided structural method to probe macromolecule–small molecule interactions, molecular docking has evolved into an essential component across various phases of drug development.

Modern drug research increasingly leverages an array of molecular modeling techniques to probe intricate biochemical systems. The integration of computational and experimental approaches has proven pivotal in the discovery and development of novel therapeutic compounds.[41] In this context, molecular docking is indispensable for analyzing ligand conformations within macromolecular binding sites and for estimating binding free energies through detailed examinations of molecular recognition processes—thereby enhancing the precision of structure-based drug design.

The curcumin analog J7 has garnered significant interest as a promising therapeutic candidate for addressing diabetic liver disease and liver fibrosis—complications that markedly impair quality of life and reduce life expectancy among diabetic patients. The advent of J7 offers a novel avenue for intervention in these disorders. Recent investigations have revealed that the pathological mechanisms underpinning diabetic liver disease and liver fibrosis involve complex, multitiered biomolecular interactions. Notably, J7 appears to exert its therapeutic effects via multiple pathways, including the modulation of inflammatory responses, reduction of oxidative stress, inhibition of hepatic stellate cell activation, and stimulation of hepatocyte regeneration.[42]

J7's therapeutic potential is largely attributed to its capacity to modulate pivotal molecular pathways implicated in the progression of diabetic liver disease and liver fibrosis. To delineate these critical pathways, we adopted a synergistic approach combining network pharmacology and molecular docking—an approach pioneered by researchers such as Kaijun Wang and Yanggang Hong.[43,44]

In particular, our analysis systematically elucidated the relationship between J7 and both diabetic liver disease and liver fibrosis, revealing that its pharmacological activity is predominantly mediated through the NF-κB and TGF-β signaling pathways, which are instrumental in modulating disease progression.

The integration of network pharmacology with molecular docking techniques has yielded profound insights into the therapeutic efficacy of J7. This research not only deepens our understanding of its mechanistic underpinnings but also lays a robust foundation for the rational design of future drug development studies, thereby advancing the scientific progression of J7 as a novel therapeutic agent.

Although our comprehensive analysis has shed light on the molecular mechanisms underlying diabetic liver disease and liver fibrosis, these findings must be contextualized within the broader framework of a global health crisis. The escalating prevalence of type 2 diabetes (T2D)—a chronic endocrine disorder marked by hyperglycemia and insulin resistance—continues to impose a significant burden, particularly through its associated liver complications, which bear high mortality rates.[45] Diabetes-induced oxidative stress, primarily due to the excessive production of superoxide anions (O_2^-), leads to increased lipid peroxidation and subsequent liver cell damage. Moreover, this oxidative milieu promotes the chemotactic recruitment of inflammatory cells, thereby exacerbating hepatic inflammation.[46,47]

Metabolic-associated fatty liver disease (MAFLD) encompasses a continuum of hepatic conditions ranging from simple steatosis to fatty hepatitis, liver fibrosis, and ultimately cirrhosis. The two-hit hypothesis, as proposed by Day, postulates that the initial insult involves hepatic fat accumulation, followed by a secondary oxidative stress event that triggers inflammation, necrosis, and fibrosis—culminating in lipid peroxidation and advanced liver fibrosis.[48–51] Prolonged exposure to elevated fatty acid levels further exacerbates liver injury by inducing the release of inflammatory mediators and cytokines, as well as exerting direct toxic effects on pancreatic β cells. This cascade also activates hepatic

stellate cells (HSCs), thereby increasing the synthesis of extracellular matrix (ECM) components, cytokines, collagenases, and their inhibitors, which collectively contribute to the progression of liver fibrosis.[52] Furthermore, hyperglycemia exacerbates hepatic damage by promoting oxidative stress, lipid peroxidation, and secondary injury, underscoring the critical importance of maintaining optimal glycemic control in mitigating diabetic liver complications.[53]

Prior studies have shown that curcumin treatment in diabetic rat models results in significant improvements in key health indicators, including fasting blood glucose, body weight, and plasma lipid peroxide levels.[54] Additionally, hyperglycemia has been implicated in the promotion of liver fibrosis through the stimulation of hepatic stellate cell activation and subsequent ECM synthesis and secretion.[55,56] In our study, the diabetic (DM) group exhibited significantly elevated levels of fasting plasma glucose (FPG), triglycerides (TG), total cholesterol (TC), and low-density lipoprotein (LDL) compared to the normal control (NC) group ($P < 0.05$). Notably, treatment with the curcumin analog J7 resulted in a significant reduction in these parameters ($P < 0.05$), suggesting that J7 is more effective than curcumin in ameliorating hyperglycemia. However, while J7 treatment improved both glycemic and lipid metabolism disorders, these parameters did not fully revert to normal levels—a finding that contrasts with previous research in db/db mice, where curcumin exhibited no significant effect on blood glucose levels.[57]

Hepatic stellate cells (HSCs) are central to the synthesis of extracellular matrix (ECM) and perform additional roles, including the storage of lipids and vitamin A.[58–61] Upon activation, HSCs transdifferentiate into myofibroblasts (MFBs) in response to signaling molecules—such as Transforming Growth Factor Beta 1 (TGF-β1), Platelet-Derived Growth Factor (PDGF), Fibroblast Growth Factor (FGF), Nerve Growth Factor (NGF), Integrin-Linked Kinase (ILK), Endothelin-1 (ET-1), and Focal Adhesion Kinase (FAK). This activation results in the overproduction of ECM components, as evidenced by the upregulation of α-smooth muscle actin (α-SMA), a hallmark of myofibroblast transformation.[62]

Our findings revealed that the DM group experienced pronounced activation of hepatic stellate cells and elevated α-SMA protein expression, correlating with increased ECM deposition. Remarkably, treatment with J7 led to a significant reduction in α-SMA expression, thereby mitigating collagen fiber formation, alleviating fibrosis, and safeguarding liver function.

Alanine aminotransferase (ALT) serves as a well-established marker of liver function, predominantly localized in the liver cytoplasm. In conditions such as non-alcoholic steatohepatitis (NASH) and hepatic necrosis, the release of intracellular ALT into the bloodstream leads to elevated serum enzyme levels. In our study, the DM group demonstrated significantly higher levels of ALT and aspartate aminotransferase (AST) compared to the normal control group ($P < 0.05$). Notably, treatment with the curcumin analog J7 resulted in a significant reduction in these enzyme levels.

Histopathological analysis employing HE staining revealed hepatic degeneration, pronounced steatosis, inflammatory cell infiltration, and varying degrees of fibrous septation in the DM group. Furthermore, Masson's trichrome staining demonstrated augmented collagen fiber proliferation and intensified green staining in the DM group relative to the normal control, indicative of fibrosis. Treatment with the curcumin analog J7, however, markedly alleviated these histopathological lesions.

Transforming Growth Factor Beta (TGF-β) plays a multifaceted role in cellular processes such as growth, differentiation, apoptosis, and immune regulation. Of its three subtypes, TGF-β1 is particularly implicated in diabetes-induced liver fibrosis and ECM production. TGF-β1 mediates its effects through the activation of Smad proteins—namely, Smad2, Smad3, and the inhibitory Smad7—which are integral to the TGF-β/Smad signaling pathway.[63] In the DM group, elevated TGF-β1 protein expression coupled with reduced Smad7 levels suggests a dysregulation of this pathway in diabetic liver fibrosis. These observations are consistent with multiple studies employing various rat models and experimental designs, which have reported similar increases in TGF-β1 expression in liver fibrosis.[64–70] Importantly, treatment with the curcumin analog J7 resulted in reduced TGF-β1 expression, thereby underscoring its potential as an anti-fibrotic agent. Moreover, our findings indicate that J7 may exhibit a superior anti-fibrotic effect relative to natural curcumin, which is already recognized for its anti-inflammatory and anti-fibrotic properties.

Nuclear factor-kappa B (NF-κB) is a pivotal transcription factor governing the expression of numerous genes, particularly those involved in inflammatory responses. In chronic liver fibrosis, NF-κB activation leads to the upregulation of α-SMA gene expression, thereby promoting hepatic stellate cell activation. Consequently, inhibition of the NF-κB

pathway can modulate the production of inflammatory mediators and downstream pro-inflammatory cytokines—including TNFα, IL-1, IL-2, IL-6, IL-8, and IL-12—as well as enzymes such as COX, LOX, MMP, and iNOS, ultimately attenuating HSC activation.[35,71–74]

Moreover, in diabetes mellitus (DM), elevated expression of NF-κB and IL-1β contributes to the upregulation of anti-apoptotic genes, inhibition of HSC apoptosis, enhanced collagen synthesis, and the progression of fibrosis. Administration of the curcumin analog J7 has been shown to downregulate IL-1β and NF-κB expression, thereby diminishing inflammatory responses and curbing liver fibrosis progression.

Apoptosis is a critical factor in the pathogenesis of liver fibrosis, with hepatocyte apoptosis contributing significantly to liver injury and regeneration. Members of the BCL-2 protein family—including the anti-apoptotic BCL-2 and the pro-apoptotic BAX—regulate apoptosis through the modulation of cytochrome C release and subsequent activation of caspase 3. The ratio of BCL-2 to BAX serves as an indicator of cellular anti-apoptotic propensity. In our DM group, a decreased BCL-2/BAX ratio coupled with elevated caspase 3 levels signified enhanced hepatocyte apoptosis. Notably, treatment with J7 elevated the BCL-2/BAX ratio and reduced caspase 3 levels, thereby inhibiting apoptosis, mitigating liver fibrosis, and preserving hepatic function. Furthermore, molecular docking studies provided insights into the interactions between J7 and the key proteins BCL-2 and BAX, with binding affinity scores of –7.416 kcal/mol and –7.617 kcal/mol, respectively—suggesting favorable binding interactions. These findings indicate that J7 may modulate immune responses in liver fibrosis by targeting apoptotic regulators, offering a novel therapeutic perspective for future research.

While gene disruption techniques or chemical inhibitors could provide additional validation for targets such as JUN or RELA, our study primarily concentrated on assessing the therapeutic efficacy of J7 and elucidating its preliminary mechanistic insights within an in vivo framework. Future investigations should consider employing siRNA knockdown or CRISPR-based strategies to isolate and confirm the specific gene effects associated with J7's action.

Conclusion

In conclusion, the curcumin analog J7 exerts beneficial effects on the liver of rats with type 2 diabetes by inhibiting liver fibrosis and protecting liver function. These effects are mediated through the inhibition of the TGF-β/Smad signaling pathway and the modulation of NF-κB, BCL-2, and BAX protein expression. J7 demonstrates its potential as a therapeutic agent for managing liver complications associated with type 2 diabetes. Further research and clinical studies are warranted to explore the full potential and mechanism of action of J7 in the treatment of liver diseases in diabetic individuals.

This study is among the first to explore the therapeutic potential of the curcumin analog J7 in the context of diabetic liver disease, highlighting its superior effects compared to traditional curcumin in attenuating liver fibrosis and regulating glucose and lipid metabolism. The findings contribute to the growing body of knowledge on curcumin analogs and their potential applications in treating metabolic disorders and associated complications.

Abbreviations

T2D - Type 2 Diabetes; IL-1β - Interleukin 1 Beta; MAFLD - Metabolic Dysfunction-Associated Fatty Liver Disease; IRS - Insulin Receptor Substrate; Akt/PKB - Protein Kinase B; HSL - Hormone-Sensitive Lipase; ATGL - Adipose Triglyceride Lipase; ACC - Acetyl-CoA Carboxylase; FAS - Fatty Acid Synthase; TNF-α - Tumor Necrosis Factor Alpha; IL-6 - Interleukin-6; α-Glucosidase - Alpha-Glucosidase; α-Amylase - Alpha-Amylase; Caco-2 - Colonic Adenocarcinoma Cells; STZ - Streptozotocin; CMC-Na - Sodium Carboxymethyl Cellulose; SD - Sprague Dawley; NC - Non-Diabetic Control; DM - Diabetes Mellitus; CUR - Curcumin; J7L - Low-Dose Curcumin Analog J7; J7H - High-Dose Curcumin Analog J7; FPG - Fasting Plasma Glucose; TG - Triglyceride; TC - Total Cholesterol; LDL-c - Low-Density Lipoprotein Cholesterol; ALT - Alanine Aminotransferase; AST - Aspartate Aminotransferase; HE - Hematoxylin and Eosin; NF-κBp65 - Nuclear Factor Kappa-Light-Chain-Enhancer of Activated B Cells p65; BCL-2 - B-Cell Lymphoma 2; BAX - BCL2-Associated X Protein; IOD - Integrated Optical Density; PBS - Phosphate Buffered Saline; ELISA - Enzyme-Linked Immunosorbent Assay; ANOVA - Analysis of Variance; TGF-β1 - Transforming Growth Factor Beta 1; TGF-β2 - Transforming Growth Factor Beta 2; TGF-β3 - Transforming Growth Factor Beta 3;

HSC - Hepatic Stellate Cells; ECM - Extracellular Matrix; α-SMA - Alpha-Smooth Muscle Actin; PDGF - Platelet-Derived Growth Factor; FGF - Fibroblast Growth Factor; NGF - Nerve Growth Factor; ILK - Integrin-Linked Kinase; ET-1 - Endothelin-1; FAK - Focal Adhesion Kinase; MFB - Myofibroblasts; TGF-βR1 - Transforming Growth Factor Beta Receptor 1; RT-PCR - Reverse Transcription Polymerase Chain Reaction; qPCR - Quantitative Polymerase Chain Reaction; COX - Cyclooxygenase; LOX - Lipoxygenase; MMP - Matrix Metallopeptidase; iNOS - Inducible Nitric Oxide Synthase; NASH - Non-Alcoholic Steatohepatitis; NF-κB - Nuclear Factor Kappa B; NK - Natural Killer; PDB - Protein Data Bank; SDS-PAGE - Sodium Dodecyl Sulfate-Polyacrylamide Gel Electrophoresis; PVDF - Polyvinylidene Fluoride; TBST - Tris-Buffered Saline Tween 20; AMPK - Adenosine Monophosphate-Activated Protein Kinase; HIF-1 - Hypoxia-Inducible Factor 1; O-2 - Superoxide Anion; SPF - Specific Pathogen-Free.

Data Sharing Statement

All data generated and/or analyzed during this study are fully included within the published article. Supplementary data related to this research can be found alongside the paper. Further information can be obtained from the corresponding author on reasonable request.

Ethics Approval

This study received comprehensive review and approval from the Institutional Review Board (IRB) at the First Affiliated Hospital of Wenzhou Medical University, fully adhering to national legislative requirements and the ethical principles outlined in the "Guidelines for Ethical Review of Laboratory Animal Welfare" (2018). Furthermore, all animal research was conducted in strict accordance with the Guide for the Care and Use of Laboratory Animals (National Academy of Sciences, published by the National Institutes of Health). Ethical approval for this study was granted by the Ethical Committee on Animal Research at the First Affiliated Hospital of Wenzhou Medical University (Approval Number: WYYY-AEC-YS-2024-0596), located in Wenzhou, Zhejiang, China.

Acknowledgments

We would like to express our deepest gratitude to Jinye Pan, Jing Zeng, and Shengyu Bao for their invaluable assistance during the revision stage of this research. Their constructive feedback and suggestions were appreciated and contributed to improving the clarity and quality of this study.

Author Contributions

All authors made substantial contributions to conception and design, acquisition of data, analysis, and interpretation of data; took part in drafting the article or revising it critically for important intellectual content; agreed to submit to the current journal; gave final approval of the version to be published; and agree to be accountable for all aspects of the work.

Funding

This research was supported by the Zhejiang Provincial Department of Education (Grant No. Y202353401), the Key Laboratory of Clinical Laboratory Diagnosis and Translational Research of Zhejiang Province (Grant No. 2022E10022) and the First Clinical Medical College of Wenzhou Medical University (Grant No. Y202352087).

Disclosure

The authors declare that they have no conflict of interest.

References

1. Rachdaoui N. Insulin: the friend and the foe in the development of type 2 diabetes mellitus. *Int J mol Sci*. 2020;21. doi:10.3390/ijms21051770
2. Badmus OO, Hillhouse SA, Anderson CD, Hinds TD, Stec DE. Molecular mechanisms of metabolic associated fatty liver disease (MAFLD): functional analysis of lipid metabolism pathways. *Clin Sci*. 1979;136:1347–1366. doi:10.1042/cs20220572
3. Sakurai Y, Kubota N, Yamauchi T, Kadowaki T. Role of insulin resistance in MAFLD. *Int J mol Sci*. 2021;22:4156. doi:10.3390/ijms22084156
4. Heeren J, Scheja L. Metabolic-associated fatty liver disease and lipoprotein metabolism. *Mol Metabol*. 2021;50:101238. doi:10.1016/j.molmet.2021.101238

5. Kotha RR, Luthria DL. Curcumin: biological, pharmaceutical, nutraceutical, *and analytical aspects*. *Molecules*; 2019;24. doi:10.3390/molecules24162930
6. Jabczyk M, Nowak J, Hudzik B, Zubelewicz-Szkodzińska B. Curcumin in metabolic health and disease. *Nutr*. 2021;13. doi:10.3390/nu13124440
7. Kasprzak-Drozd K, Oniszczuk T, Gancarz M, et al. Curcumin and weight loss: does it work? *Int J mol Sci*. 2022;23:639. doi:10.3390/ijms23020639
8. Iranshahy M, Hanafi-Bojd MY, Aghili SH, et al. Curcumin-loaded mesoporous silica nanoparticles for drug delivery: synthesis, biological assays and therapeutic potential - a review. *RSC Adv*. 2023;13(32):22250–22267. doi:10.1039/d3ra02772d
9. Chainoglou E, Hadjipavlou-Litina D. Curcumin analogues and derivatives with anti-proliferative and anti-inflammatory activity: structural characteristics and molecular targets. *Expert Opin Drug Discov*. 2019;14:821–842. doi:10.1080/17460441.2019.1614560
10. Noureddin SA, El-Shishtawy RM, Al-Footy KO. Curcumin analogues and their hybrid molecules as multifunctional drugs. *Eur J Med Chem*. 2019;182:111631. doi:10.1016/j.ejmech.2019.111631
11. Huang L, Xie D, Yu Y, et al. TCMID 2.0: a comprehensive resource for TCM. *Nucleic Acids Res*. 2018;46:D1117–d1120. doi:10.1093/nar/gkx1028
12. Xu HY, Zhang Y-Q, Liu Z-M, et al. ETCM: an encyclopaedia of traditional Chinese medicine. *Nucleic Acids Res*. 2019;47:D976–d982. doi:10.1093/nar/gky987
13. Daina A, Michielin O, Zoete V. SwissTargetPrediction: updated data and new features for efficient prediction of protein targets of small molecules. *Nucleic Acids Res*. 2019;47:W357–w364. doi:10.1093/nar/gkz382
14. Davis AP, Wiegers TC, Johnson RJ, et al. Comparative Toxicogenomics Database (CTD): update 2023. *Nucleic Acids Res*. 2023;51:D1257–d1262. doi:10.1093/nar/gkac833
15. Paz-Pacheco E. Going PubMed, Writing Together! *J ASEAN Fed Endocr Soc*. 2023;38(4):4. doi:10.15605/jafes.038.01.01
16. Amberger JS, Hamosh A. Searching online mendelian inheritance in man (Omim): a knowledgebase of human genes and genetic phenotypes. *Curr protoc bioinf*. 2017;58:1.2.1–1.2.12. doi:10.1002/cpbi.27
17. Stelzer G, Rosen N, Plaschkes I, et al. The genecards suite: from gene data mining to disease genome sequence analyses. *Curr protoc bioinf*. 2016;54:1.30.31–31.30.33. doi:10.1002/cpbi.5
18. Szklarczyk D, Kirsch R, Koutrouli M, et al. The STRING database in 2023: protein-protein association networks and functional enrichment analyses for any sequenced genome of interest. *Nucleic Acids Res*. 2023;51:D638–d646. doi:10.1093/nar/gkac1000
19. Karuppasamy MP, Venkateswaran S, Subbiah P. PDB-2-PBv3.0: an updated protein block database. *J Bioinf Comput Biol*. 2020;18:2050009. doi:10.1142/s0219720020500092
20. Kim S, Chen J, Cheng T, et al. PubChem in 2021: new data content and improved web interfaces. *Nucleic Acids Res*. 2021;49:D1388–d1395. doi:10.1093/nar/gkaa971
21. Liu Y, Yang X, Gan J, et al. CB-Dock2: improved protein-ligand blind docking by integrating cavity detection, docking and homologous template fitting. *Nucleic Acids Res*. 2022;50:W159–w164. doi:10.1093/nar/gkac394
22. Schriml LM, Munro JB, Schor M, et al. The human disease ontology 2022 update. *Nucleic Acids Res*. 2022;50:D1255–d1261. doi:10.1093/nar/gkab1063
23. Gene Ontology Consortium: going forward. *Nucleic Acids Res*. 2015;43:D1049–1056. doi:10.1093/nar/gku1179
24. Kanehisa M, Goto S. KEGG: kyoto encyclopedia of genes and genomes. *Nucleic Acids Res*. 2000;28:27–30. doi:10.1093/nar/28.1.27
25. Ghasemi A, Jeddi S. Streptozotocin as a tool for induction of rat models of diabetes: a practical guide. *EXCLI J*. 2023;22:274–294.PMID: 36998708. doi:10.17179/excli2022-5720
26. Furman BL. Streptozotocin-induced diabetic models in mice and rats. *Curr Protoc*. 2021;1:e78.PMID: 33905609. doi:10.1002/cpz1.78
27. Southam K, de Sousa C, Daniel A, Taylor BV, Foa L, Premilovac D. Development and characterisation of a rat model that exhibits both metabolic dysfunction and neurodegeneration seen in type 2 diabetes. *J Physiol*. 2022;600:1611–1630.PMID: 35128667. doi:10.1113/JP282454
28. Reed MJ, Meszaros K, Entes LJ, et al. A new rat model of type 2 diabetes: the fat-fed, streptozotocin-treated rat. *Metabolism*. 2000;49:1390–1394. PMID: 11092499. doi:10.1053/meta.2000.17721
29. Xu FF, Miao CF, Chi C, Wu G, Chen GR. Intervention of curcumin and its analogue J7 on oxidative stress injury in testis of type 2 diabetic rats. *Zhongguo Ying Yong Sheng Li Xue Za Zhi*. 2019;35:145–149.PMID: 31250606. doi:10.12047/j.cjap.5783.2019.032
30. Gagea-Iurascu M, Craig S. Euthanasia and Necropsy. In: *The Laboratory Rabbit*. Guinea Pig, Hamster, and Other Rodents. Elsevier; 2012:117–139.
31. Guidelines for the euthanasia of animals. American Veterinary Medical Association. Available from: https://www.avma.org/resources-tools/avma-policies/avma-guidelines-euthanasia-animals. Accessed March 27, 2025.
32. Malatesta M. Histological and histochemical methods - theory and practice. *Eur J Histochem*. 2016;60. doi:10.4081/ejh.2016.2639
33. Ramos-Vara JA. Technical aspects of immunohistochemistry. *Vet Pathol*. 2005;42:405–426.PMID: 16006601. doi:10.1354/vp.42-4-405
34. Chen Y, et al. Correction: the chemerin/CMKLR1 axis is involved in the recruitment of microglia to Aβ Deposition through p38 MAPK pathway. *Int J Mol Sci*. 2022;23:9041. doi:10.3390/ijms23169041
35. Alvarenga L, Salarolli R, Cardozo LFMF, et al. Impact of curcumin supplementation on expression of inflammatory transcription factors in hemodialysis patients: a pilot randomized, double-blind, controlled study. *Clin Nutr*. 2020;39:3594–3600. doi:10.1016/j.clnu.2020.03.007
36. Srinivasan K, Viswanad B, Asrat L, Kaul CL, Ramarao P. Combination of high-fat diet-fed and low-dose streptozotocin-treated rat: a model for type 2 diabetes and pharmacological screening. *Pharmacol Res*. 2005;52:313–320.PMID: 15979893. doi:10.1016/j.phrs.2005.05.004
37. Nogales C, Mamdouh ZM, List M, et al. Network pharmacology: curing causal mechanisms instead of treating symptoms. *Trends Pharmacol Sci*. 2022;43:136–150. doi:10.1016/j.tips.2021.11.004
38. Hopkins AL. Network pharmacology: the next paradigm in drug discovery. *Nat Chem Biol*. 2008;4:682–690. doi:10.1038/nchembio.118
39. Chicco D, Jurman G. A brief survey of tools for genomic regions enrichment analysis. *Front Bioinform*. 2022;2:968327. doi:10.3389/fbinf.2022.968327
40. Sahu D, Rathor LS, Dwivedi SD, et al. A review on molecular docking as an interpretative tool for molecular targets in disease management. *ASSAY Drug Dev Technol*. 2024;22:40–50. doi:10.1089/adt.2023.060
41. Danel T, Łęski J, Podlewska S, Podolak IT. Docking-based generative approaches in the search for new drug candidates. *Drug Discov Today*. 2023;28:103439. doi:10.1016/j.drudis.2022.103439
42. Xu FF, Miao CF, Chi C, Wu G, Chen GR. Intervention of curcumin and its analogue J7 on oxidative stress injury in testis of type 2 diabetic rats. *Zhongguo Ying Yong Sheng Li Xue Za Zhi*. 2019;35:145–149. doi:10.12047/j.cjap.5783.2019.032

43. Hong Y, Wang D, Lin Y, et al. Environmental triggers and future risk of developing autoimmune diseases: molecular mechanism and network toxicology analysis of bisphenol A. *Ecotoxicol Environ Saf*. 2024;288:117352. doi:10.1016/j.ecoenv.2024.117352
44. Wang K, Yin J, Chen J, et al. Inhibition of inflammation by berberine: molecular mechanism and network pharmacology analysis. *Phytomedicine*. 2024;128:155258. doi:10.1016/j.phymed.2023.155258
45. Russo MP, Grande-Ratti MF, Burgos MA, Molaro AA, Bonella MB. Prevalence of diabetes, epidemiological characteristics and vascular complications. *Archivos de cardiologia de Mexico*. 2023;93:30–36. doi:10.24875/acm.21000410
46. Reed J, Bain S, Kanamarlapudi V. A review of current trends with type 2 diabetes epidemiology, aetiology, pathogenesis, treatments and future perspectives. *Diabetes Metab Syndr Obes*. 2021;14:3567–3602. doi:10.2147/dmso.S319895
47. Darenskaya MA, Kolesnikova LI, Kolesnikov SI. Oxidative stress: pathogenetic role in diabetes mellitus and its complications and therapeutic approaches to correction. *Bull Exp Biol Med*. 2021;171:179–189. doi:10.1007/s10517-021-05191-7
48. Pipitone RM, Ciccioli C, Infantino G, et al. MAFLD: a multisystem disease. *Her Adv Endocrinol Metab*. 2023;14:20420188221145549. doi:10.1177/20420188221145549
49. Kawaguchi T, Tsutsumi T, Nakano D, Torimura T. MAFLD: renovation of clinical practice and disease awareness of fatty liver. *Hepatol Res*. 2022;52:422–432. doi:10.1111/hepr.13706
50. Sangro P, de la Torre Aláez M, Sangro B, D'Avola D. Metabolic dysfunction-associated fatty liver disease (MAFLD): an update of the recent advances in pharmacological treatment. *J Physiol Biochem*. 2023;79. doi:10.1007/s13105-023-00954-4
51. Kaya E, Yilmaz Y. Metabolic-associated Fatty Liver Disease (MAFLD): a Multi-systemic Disease beyond the liver. *J clin transl hepatol*. 2022;10:329–338. doi:10.14218/jcth.2021.00178
52. Dong Q, Bao H, Wang J, et al. Liver fibrosis and MAFLD: the exploration of multi-drug combination therapy strategies. *Front Med*. 2023;10:1120621. doi:10.3389/fmed.2023.1120621
53. Caussy C, Aubin A, Loomba R. the relationship between type 2 diabetes, NAFLD, and cardiovascular risk. *Current Diabetes Rep*. 2021;21:15. doi:10.1007/s11892-021-01383-7
54. Belhan S, Yıldırım S, Huyut Z, et al. Effects of curcumin on sperm quality, lipid profile, antioxidant activity and histopathological changes in streptozotocin-induced diabetes in rats. *Andrologia*. 2020;52:e13584. doi:10.1111/and.13584
55. Zhang H, Chen F, Fan X, et al. Quantitative proteomic analysis on activated hepatic stellate cells reversion reveal STAT1 as a key regulator between liver fibrosis and recovery. *Sci Rep*. 2017;7:44910. doi:10.1038/srep44910
56. Higashi T, Friedman SL, Hoshida Y. Hepatic stellate cells as key target in liver fibrosis. *Adv Drug Delivery Rev*. 2017;121:27–42. doi:10.1016/j.addr.2017.05.007
57. Zhong J, Gong W, Chen J, et al. Micheliolide alleviates hepatic steatosis in db/db mice by inhibiting inflammation and promoting autophagy via PPAR-γ-mediated NF-κB and AMPK/mTOR signaling. *Int Immunopharmacol*. 2018;59:197–208. doi:10.1016/j.intimp.2018.03.036
58. Shang L, Hosseini M, Liu X, Kisseleva T, Brenner DA. Human hepatic stellate cell isolation and characterization. *J Gastroenterol*. 2018;53:6–17. doi:10.1007/s00535-017-1404-4
59. Eun K, Ham SW, Kim H. Cancer stem cell heterogeneity: origin and new perspectives on CSC targeting. *BMB Reports*. 2017;50:117–125. doi:10.5483/bmbrep.2017.50.3.222
60. Senoo H, Mezaki Y, Fujiwara M. The stellate cell system (vitamin A-storing cell system). *Anat Sci Int*. 2017;92:387–455. doi:10.1007/s12565-017-0395-9
61. Rezaii M, Oryan S, Javeri A. Curcumin nanoparticles incorporated collagen-chitosan scaffold promotes cutaneous wound healing through regulation of TGF-β1/Smad7 gene expression. *Mater Sci Eng C Mater Biol Appl*. 2019;98:347–357. doi:10.1016/j.msec.2018.12.143
62. Chen H, Gan Q, Yang C, et al. A novel role of glutathione S-transferase A3 in inhibiting hepatic stellate cell activation and rat hepatic fibrosis. *J Transl Med*. 2019;17:280. doi:10.1186/s12967-019-2027-8
63. Akhurst RJ. Targeting TGF-β signaling for therapeutic gain. *Cold Spring Harb Perspect Biol*. 2017. doi:10.1101/cshperspect.a022301
64. Elkattawy HA, Elsherbini DM, Ebrahim HA, et al. Rho-kinase inhibition ameliorates non-alcoholic fatty liver disease in type 2 diabetic rats. *Physiol Res*. 2022;71:615–630. doi:10.33549/physiolres.934869
65. Lee H, Lee H, Lim Y. Vitamin D(3) improves lipophagy-associated renal lipid metabolism and tissue damage in diabetic mice. *Nut Res*. 2020;80:55–65. doi:10.1016/j.nutres.2020.06.007
66. Peng X, Dai C, Liu Q, Li J, Qiu J. Curcumin attenuates on carbon tetrachloride-induced acute liver injury in mice via modulation of the Nrf2/HO-1 and TGF-B1/Smad3 pathway. *Molecules*. 2018;23. doi:10.3390/molecules23010215
67. Wang X, Sun X, Abulizi A, et al. Effects of salvianolic acid A on intestinal microbiota and lipid metabolism disorders in Zucker diabetic fatty rats. *Diabetol Metab Syndr*. 2022;14:135. doi:10.1186/s13098-022-00868-z
68. Borém LMA, Neto JFR, Brandi IV, Lelis DF, Santos SHS. The role of the angiotensin II type I receptor blocker telmisartan in the treatment of non-alcoholic fatty liver disease: a brief review. *Hypertens Res*. 2018;41:394–405. doi:10.1038/s41440-018-0040-6
69. Tutunchi H, Ostadrahimi A, Saghafi-Asl M, Maleki V. The effects of oleoylethanolamide, an endogenous PPAR-α agonist, on risk factors for NAFLD: a systematic review. *Obesity Rev*. 2019;20:1057–1069. doi:10.1111/obr.12853
70. Kefala G, Tziomalos K. Apoptosis signal-regulating kinase-1 as a therapeutic target in nonalcoholic fatty liver disease. *Expert Rev Gastroenterol Hepatol*. 2019;13:189–191. doi:10.1080/17474124.2019.1570136
71. Bangham CRM, Matsuoka M. Human T-cell leukaemia virus type 1: parasitism and pathogenesis. *Philos Trans R Soc London Ser B*. 2017;372. doi:10.1098/rstb.2016.0272
72. Meiyanto E, Septisetyani EP, Larasati YA, Kawaichi M. Curcumin analog pentagamavunon-1 (PGV-1) sensitizes widr cells to 5-Fluorouracil through Inhibition of NF-κB activation. *Asian Pac J Cancer Prev*. 2018;19:49–56. doi:10.22034/apjcp.2018.19.1.49
73. Grassin-Delyle S, Abrial C, Salvator H, et al. The role of toll-like receptors in the production of cytokines by human lung macrophages. *J Innate Immun*. 2020;12:63–73. doi:10.1159/000494463
74. Pickich MB, Hargrove MW, Phillips CN, et al. Effect of curcumin supplementation on serum expression of select cytokines and chemokines in a female rat model of nonalcoholic steatohepatitis. *BMC Res Notes*. 2019;12:496. doi:10.1186/s13104-019-4540-5